Determining Seasonal Spatial and Temporal Distribution of Chlorophyll-a, and its Concentration in Kuwait and the Arabian Gulf Using Satellite and In-situ Data

Jasem A Albanai

As an indicator of phytoplankton density in an area, the concentration of chlorophyll-a (Chl-a) is an important reflection of marine water quality. Remote sensing techniques have been developed to measure the near-surface concentration of Chl-a in water by combining spectral bands and in situ data. This algorithm can be applied to sensors of varying spatial, temporal and spectral resolutions. However, in this study, Chl-a level 2 and 3 products of SNPP – VIIRS spectrometer (Equation OC3) from NASA's OceanColor suite were relied upon to establish the spatial and temporal distribution of Chl-a concentration in the Arabian Gulf (also known as the Persian Gulf) and the territorial waters of the State of Kuwait (located in the north-eastern part of the Arabian Gulf) in 2012-2019. Ground truthing points (n = 192) matched with level 2 products have been used to build and cross-validate an empirical model. The correlation was positive, with r^2 = 0.79 and validation RMSE = ± 0.64 mg/m-3. The derived algorithm was then applied to Chl-a level 3 seasonal products. Additionally, the Chl-a concentration values in Kuwaiti waters were enhanced using the IDW algorithm to increase spatial resolution, given its small size compared to the spatial resolution of level 3 Chl-a products. The model derived from IDW was tested using the Mann Whitney test (Sig = 0.948 p > 0.01). However, the result showed that Chl-a concentration was higher in the Kuwait Bay (average = 2.8 mg/m-3) than in Kuwaiti waters (average = 2.3 mg/m-3), and higher in Kuwaiti waters (average = 2.1 mg/m-3) than in the Arabian Gulf (average = 0.7 mg/m-3). Coasts have higher concentrations than open water. Generally, the Chl-a increases in winter and had a semi-regular cycle during the years of study; this cycle is more regular in the Gulf than in Kuwait.

KEY WORDS
~ Geography
~ Biogeography
~ GIS
~ OceanColor
~ VIIRS

University of Oxford, School of Geography and the Environment, Oxford, United Kingdom
e-mail: albanay.com@gmail.com
doi: 10.7225/toms.v13.n02.016

Received: 10 Jul 2023 / Revised: 30 Jun 2024 / Accepted: 12 Sep 2024 / Published: 21 Oct 2024

1. INTRODUCTION

Sea and ocean water quality is determined based on its physical, chemical and biological properties, such as sea temperature, salinity, dissolved oxygen, pH and Chl-a concentration, among others. One of the most valuable approaches in studying water quality is the analysis of the temporal and spatial distribution of marine variables, and the measurement of the changes in these patterns. Chl-a concentration is an indicator of phytoplankton density (Muller-Karger et al., 2005) which can help monitor and assess marine resources and water quality (Al-naimi et al., 2017). Remote sensing techniques have been widely used to obtain marine quality parameters (Al-Rashidi et al., 2009; Cahyono et al., 2017; Huang et al., 2014; Mutlow et al., 1994; Thomas et al., 2002). Chl-a data for large geographic areas can be obtained systematically through remote sensing instruments, rather than through the use of field-point observations (Jensen, 2016). Statistical methods have been used extensively in literature to describe and analyse the temporal and spatial distribution of marine water quality parameters using remote sensing methods and field surveys (Williams et al., 2013; Yoder et al., 2001). Several methods have been used to determine Chl-a concentrations from space. While some focus on stationary variation, such as using the Empirical Orthogonal Function (Williams et al., 2013) which analyses the spatio-temporal variation with a set of orthogonal functions, others focus on non-stationary variation methods (Mendonça et al., 2010; Zhang et al., 2012) which highlight sudden changes due to abnormal events (Moradi and Kabiri, 2015), more often than not controlled by hydrodynamics, bathymetry, stratification, mixing processes and nutrient uptake (Glibert et al., 2002; Moradi and Kabiri, 2012). Therefore, both stationary and non-stationary variations contribute to our understanding of the spatial and temporal distribution of Chl-a concentration (Moradi and Kabiri, 2015).

Studies attempting to extract marine environment parameters in the Arabian Gulf from satellites are few and far between, despite their global relevance and importance, mainly due to dust storms that obstruct the operation of remote sensing instruments (Nezlin et al., 2010; Zhao and Ghedira, 2014), the lack of quality in-situ measurements, complex sea-river environments (Al-naimi et al., 2017), and the limited spatial coverage of many global remote sensing products over the marginal seas of the Arabian Gulf. However, the general water circulation, bathymetry and hydrodynamics in the Arabian Gulf have been discussed and analysed by numerous authors (Brewer and Dyrssen, 1985; Nezlin et al., 2010; Reynolds, 1993, 1993; Sheppard et al., 2010). Nezlin et al. (2007) divided the Gulf into regions based on oceanographic properties and water circulation (Reynolds, 1993), estimating that the Chl-a concentration is much higher in the northern part of the Gulf. Lately, remote sensing instruments have been widely used to obtain near-surface Chl-a concentrations, measured by moderate spatial resolution satellites provided by NASA through the correlation of blue-to-green spectral range and in-situ data (O'Reilly et al., 1998). As to the benefits of remote sensing methods, Reilly et al. (2000) showed that remote sensing could be affected by bottom reflection and high turbidity. The NASA OceanColor products were developed to measure Chl-a in open oceans, where water color mainly depends on Chl-a concentration (Reilly et al., 2000). The Arabian Gulf is classified as a marginal water, influenced by the discharge of the Tigris and the Euphrates, which means that Chl-a concentration is affected by the concentrations of both dissolved and suspended matter (Siegel et al., 2005). In such circumstances, regional models for the Arabian Gulf give more accurate results (Nezlin et al., 2007).

Nezlin et al. (2010) derived the monthly Chl-a concentration, and analysed environmental factors relevant for phytoplankton distribution. The study showed that the Chl-a concentration peaks in August and October, and hits minimum in February and March. The field-based measurements of Chl-a show that the concentration ranges from 0.01 to 10 mg/m^{-3} in the Arabian Gulf (Sheppard et al., 2010), and up to 55.4 to 4525 mg/m^{-3} in abnormal bloom conditions in the northwest of the Gulf (Al-Yamani et al., 2012). Moradi and Kabiri (2015) studied the spatial and temporal variation of Chl-a in 2002-2013 using MODIS data. Their study showed that the stationary level of Chl-a concentration is higher in coastal areas, while the temporal peaks can be noticed in summer and winter in the north-western region. However, the accuracy of VIIRS and other merged satellites sensors' datasets in measuring Chl-a concentration were validated positively in the Arabian Gulf by Al-naimi et

al. (2017) through ground truthing points taken in the mid-west of the Gulf. Additionally, Zhao et al. (Zhao et al., 2016) developed and tested the red tide index over the Arabian Gulf using the MODIS Aqua satellite sensor, while Polikarpov et al. (2019) discussed the phytoplankton variability over the Arabian Gulf, also using the MODIS Aqua satellite sensor.

As for the northern reaches of the Arabian Gulf, the territorial waters of Kuwait are in the west. Studies looking at the spatial and temporal distribution of Chl-a concentration are limited to Alyamani et al. (2004) study. In their comprehensive analysis of Kuwait's marine environment, the authors show the spatial-temporal variation of Chl-a in Kuwaiti waters based on field measurements from Kuwait Environmental Public Authority. The study showed that the concentration of Chl-a decreases from north to south, with the concentration being much higher in the north and in the Kuwait Bay during the winter and early spring. Given the small number of studies conducted in Kuwaiti waters specifically, there is a need to clarify the spatial-temporal difference. Therefore, this study aims to contribute to our understanding of the spatial-temporal Chl-a distribution based on empirical spatial enhancements of VIIRS - SNPP data for Kuwaiti waters as a part of the Arabian Gulf. The distribution and dynamics of Chl-a concentration in Kuwaiti waters is the key indicator for understanding phytoplankton density, as well as Kuwait's marine ecosystem environment, from both spatial and temporal perspective. Additionally, VIIRS is seen as a MODIS successor in providing geophysical data with higher spatial resolution (Feldman, 2020b). The two sensors differ slightly in the green, blue and red spectral bands used in the final products of NASA's OceanColor (Feldman, 2020a). However, in several studies, VIIRS showed a lower average error than MODIS in measuring Chl-a concentration, using an OC3 algorithm, across different regions of the world (including the Gulf of Gabes, the northern South China Sea, the Red Sea, the California Current Bed and the Arabian Gulf) (Al-naimi et al., 2017; Brewin et al., 2013; Hattab et al., 2013; Kahru et al., 2014; Shang et al., 2014). Therefore, using VIIRS on the North Arabian Gulf will increase our understanding of the satellite response in order to obtain measurements for both Chl-a concentration and phytoplankton density.

2. STUDY AREA

2.1. Arabian Gulf

The Arabian Gulf (also known as the Persian Gulf) is a shallow marginal sea of the Indian Ocean (Fig. 1), between the Arabian Peninsula and south-western Iran (J. A. Albanai, 2021a). The Gulf is located between 23.5° and 30.05° North and 47.5° and 56.4° East, approximately 56 km in length – 338 km in width, covering the total surface area of 240,000 km^2 (Alyamani et al., 2004; Pokavanich et al., 2014; Polikarpov et al., 2019). The total water volume in the Gulf is estimated to be roughly 6000 km^3 (Moradi and Kabiri, 2015). The Gulf is relatively shallow, with the deepest point reaching just over 100m, and the average depth of about 35m. The main source of fresh water comes from the Shatt al-Arab deltaic system (the delta of Tigris, Euphrates and Karun rivers) in the northern end of the Gulf. The maximum discharge occurs in late spring and early summer (Alyamani et al., 2004). The quantity of material discharged into the Gulf by the main northern rivers is estimated to be 1.1 * 10^8 m^3 of water and 4.8 * 10^6 tons of sediment annually (Reynolds, 1993). The Gulf is connected to the Arabian Sea and the Indian Ocean by the Strait of Hormuz, allowing the slow circulation of water (Hunter, 1983). The mean hydrodynamic circulation is counter-clockwise cyclonic, forced with the inflowing currents to the north of the Gulf in summer, and weakened by the north-westerly winds along the Iranian coast in winter (Reynolds, 1993). The Arabian Gulf has a subtropical hyper-arid climate and is surrounded by deserts, where precipitation levels are relativity limited (Alyamani et al., 2004), and evaporation rate is estimated by numerous authors to be very high (1.44 - 1.64 m year^{-1}) (Johns et al., 2003).

The physiochemical properties of Gulf's waters reflect the shallowness, high evaporation, limited freshwater river runoff and low rainfall. Sea surface temperature reaches the maximum of roughly 36°C and the minimum of 14°C (Albanai, 2022). The Arabian Gulf is considered to be one of the most saline basins in the Earth. The salinity concentration ranges from 35-40 PSU, reaching 70 PSU in shallow south-eastern

embayments (Al-naimi et al., 2017; Polikarpov et al., 2019; Reynolds, 1993). The deeper parts of the Gulf have an evident saline stratification, while the shallows are well mixed by both the wind and current systems. The north-westerly winds and south-eastward coastal currents cause the upwelling along the eastern Iranian coasts and downwelling along the western Arabian coasts (Reynolds, 1993). The recent study by Al-Yamani and Naqvi (2019) showed an increase in salinity in the northern part of the Gulf due to reduced river runoff. The Gulf is one of the main sources of aeolian dust deposits in the world (Husar et al., 1997). Belt dust storms intensify in the summer, with the strong dust-laden north-western winds which ease in the winter (Nezlin et al., 2010; Zhao and Ghedira, 2014). There is a strong correlation between the biological productivity in the Arabian Gulf and the geographical distribution of nutrients (Polikarpov et al., 2019). The limited upwelling conditions in the Gulf result in a limited nutrient concentration in most offshore Gulf waters (Johns et al., 2003); by contrast, some coastal river-discharge-influenced areas have much higher nutrient concentrations (Polikarpov et al., 2016). However, a significant increase in nutrients has been identified (J. A. Albanai, 2021b), chiefly attributable to the sewage discharge from the urban coastal areas along Gulf's coasts. Recently, the anthropogenic stresses have been cited as one of the biggest challenges facing the marine ecological environment of the Arabian Gulf (Al-Yamani and Naqvi, 2019). Nezlin et al. (2007) have divided the Gulf into regional sub-basins depending on properties, and a more recent study by ((Polikarpov et al. 2019) sought to modify this partition (Fig. 1). The Arabian Gulf is of great economic and international importance due to the transportation of oil through the Strait of Hormuz (Kvenvolden and Cooper, 2003), in addition to the Gulf's highly productive ecosystems (Polikarpov et al., 2019).

2.2. Kuwait

Kuwait is a state situated in the north-western corner of the Arabian Gulf, surrounded by Saudi Arabia to the south and west, and Iraq to the north. Kuwait is part of the Arabian desert and is considered one of the warmest regions in the world. Summer temperatures go above 50°C, and drop to about 7°C in the winter (Albanai, 2021). The flat topography of Kuwait plays a role in the drought; the elevation rises from sea level on the eastern coasts to the highest point in the south-east of the country, reaching up to 280 meters above sea level (Albanai, 2019). Kuwaiti waters are considered to be a part of the submerged northern estuarine flat of the Arabian Gulf (Fig. 1), which is mainly affected by the sea-river environment of Shatt al-Arab (Alyamani et al., 2004). The length of the State of Kuwait's coastline is more than 700 km (Misak et al., 2003). This length has, in recent years, increased due to various development projects and the construction of artificial beaches. Kuwait has nine islands (Albanai, 2021d, 2021c). Physiographically, these islands can be classified into two groups: coastal and offshore (Alyamani et al., 2004). The coastal group consists of six islands located in the north of the country's territorial waters. These are Warba, Bubyan, Miskan, Failaka, Awhah and Umm Al-Namil. A narrow channel called Khor Al-Sabbiya separates Bubyan and Warba from the mainland of the State of Kuwait. The remaining the islands of Kubber, Qaruh and Amm Al-Maradim are located in the country's southern waters (Albanai et al., 2022b).

Kuwait's territorial waters, having the surface of about 8,000 square kilometres (Albanai et al., 2022a), are divided into three main sub-regions: Kuwait Bay, the northern waters, and the southern waters. Kuwait Bay is located in the middle of the country's coastline. The bay is shallow, with the average depth of about five meters; a slow counterclockwise circulation appears in Kuwait Bay throughout much of the year while, in winter, the circulation is significantly reversed due to the predominant south-easterly (Alyamani et al., 2004). Kuwait Bay has other different sub-circulation patterns, such as the net clockwise drift in the west, and the counter-clockwise pattern in the east (Dames and Moore, 1983). As for the northern region, it is characterized by a narrow channel surrounding Warba and Bubyan islands, which makes the currents the main hydrodynamic factor in the region (El-Baz and Al-Sarawi, 2000). Maximum current speeds were observed in Khor Al-Subbiya (1.2 meters s^{-2}) (Alyamani et al., 2004). Northern waters are a part of the submerged northern estuarine flat, while southern waters are more similar to those of the open Arabian Gulf (Albanai, 2020). Here, maximum depth increases to approx. 30 meters, which makes the average depth of Kuwaiti waters about 20 meters (Alyamani

et al., 2004). Kuwait's territorial waters have the average sea surface temperature of 23.8°C and salinity of around 40 PSU (Alyamani et al., 2004).

The study area was chosen for many reasons: 1) it has high concentrations of Chl-a compared to other seas in the world, 2) the study area is exposed to strong human influence, which provides an opportunity to examine the potential connections between human factors and the natural environment, 3) the availability and access to field data for the study area which are important for remote sensing data validation.

3. METHODOLOGY

3.1. In-situ data

The field data used have been obtained from the Kuwait Environmental Public Authority (KEPA) (epa.org.kw). KEPA has been keeping a data archive on Kuwait's marine environment since 1983. In 2016, KEPA established a marine monitoring system using 15 buoys spread across Kuwaiti territorial waters (Fig. 1). Three buoys are located in the northern waters (S1 - S3), five in the Kuwait Bay (S4 – S8), while the rest can be found in the southern waters (S9 – S15). The buoy coordinates are available on KEPA website. The archive comprises data on multiple water quality parameters, such as sea surface temperature, salinity, conductivity and turbidity, dissolved oxygen and pH. The Chl-a was measured by the Turner CYCLOPS-7 (Model SEN-CHA-XAN-06) sensor. Instruments are calibrated annually, and periodically, 15-30 days after the field visit. Calibration is conducted in keeping with the NIST standard. Readings are taken every 10 minutes, at the depth of 0.5-1 m from the surface. The instrument has occasionally malfunctioned, causing some gaps in readings.

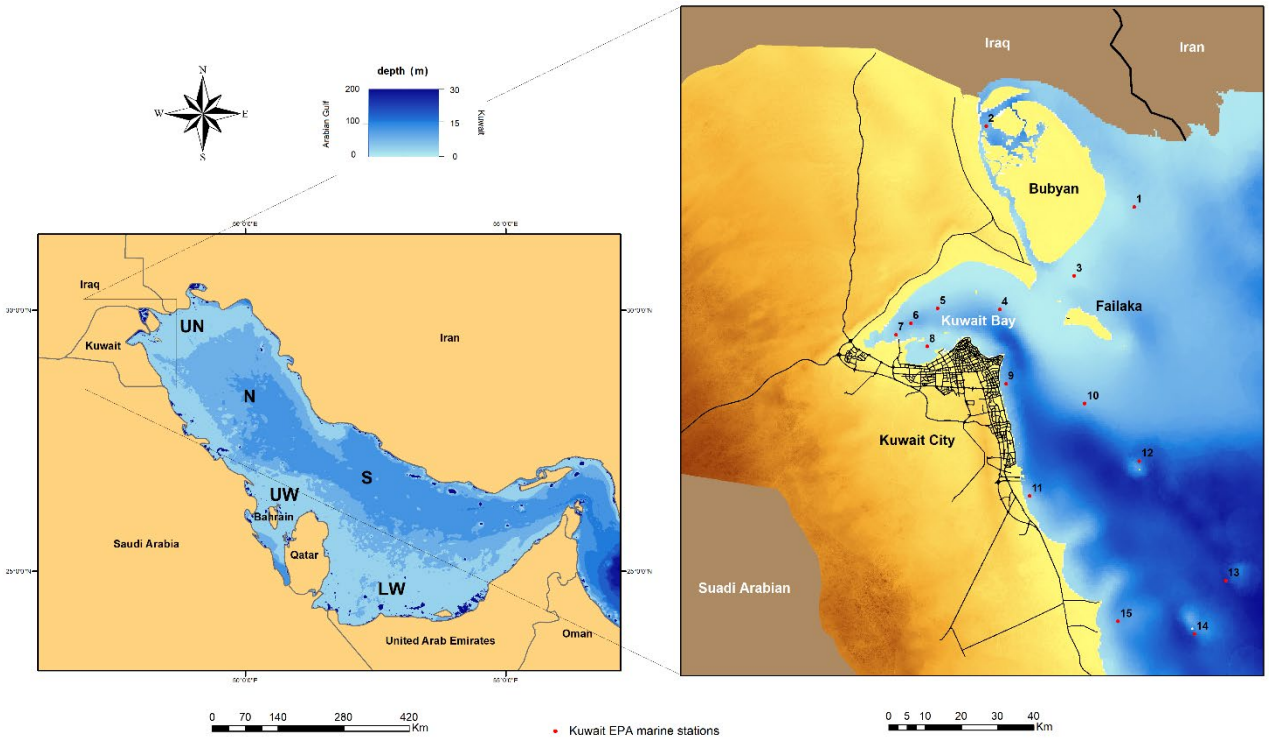

Figure 1. The Arabian Gulf (with sub-basin regions): the upper coastal Northern Shatt Al-Arab zone (UN), the northern open waters (N), the southern open waters (S), upper coastal western Saudi Arabian zone (UW), and the lower shallow waters between Qatar and UAE, including Bahrain's coasts (LW). On the right are the locations of Kuwaiti waters and Environmental Public Authority marine buoys. According to Polikarpov et al. (2019) with modifications

The Chl-a data as measured by the 15 buoys at 10:00 – 11:00 AM (hourly average) throughout 2017 have been used in the study as ground truthing points (GTPs). Additionally, turbidity data (measured by AML oceanographic sensor model XCH-TRB-A3000-02W) were used to understand the optical properties in different studied parts of Kuwait's waters, and a bathymetric layer obtained from the admiralty chart of Kuwaiti territorial waters, referred to the Ministry of Defence and the Ministry of Communications archived by KEPA, was used to show the bathymetry of Kuwait territorial waters.

3.2. Satellite data

The data used have been downloaded from the OceanColor website (oceancolor.gsfc.nasa.gov). NASA OceanColor is a platform supported by the Ocean Biology Processing Group (OBPG) at NASA's Goddard Space Flight Center. Since 1996, NASA has supported the scientific community with different products that relate to the marine environment and water quality, using satellite data. The products are divided into levels. Generally, level 1 and 2 data contain full-resolution, time-referenced and radiometrically- and geometrically-calibrated data, as well as derived geophysical variables such as sea surface temperature and Chl-a concentration. On the other hand, level 3 data contain time-derived geophysical variables over a specific period (monthly, annually etc.). The OceanColor website provides data for several sensors, such as SeaWiFS, Aquarius, MODIS and VIIRS. The Visible and Infrared Imager/Radiometer Suite (VIIRS) is a spectrometer carried by the Suomi National Polar-orbiting Partnership (S-NPP) launched in October 2011, which is being orbited on the Joint Polar Satellite System (JPSS). VIIRS is a moderate-resolution spectrometer with 22 spectral bands, ranging from 412 μm to 12 μm; 16 bands have the spatial resolution of 750m at their lowest, while five image resolution bands have the spatial resolution of 375m, and there is one day-night band (DNB) (Feldman, 2020b; Gallegos et al., 2015). The spectrometer obtained the geophysical variables of near-surface concentration of Chl-a in mg/m^{-3} using an empirical correlation between the blue to green bands ratios of spectral reflections depending on two to four bands, ranging between 440 and 570 μm, and in-situ measurements (Feldman, 2020a). The band ratio algorithm developed by O'Reilly et al. (1998) was merged with a prior water index algorithm developed by Hu et al. (2012) to produce the final product provided by NASA. Hu et al. (2012) clearly show that the improvement is limited to relativity clear water. The algorithm applied slightly differs from that published in their paper because the transition between the water color index (CI) and the band rationing algorithm (OCx) now occurs at 0.15 < CI < 0.2 mg/m^{-3} to ensure smooth transition (Feldman, 2020a). The current Chl-a product is based on the following algorithms:

$$CI = R_{rs}(\lambda_{green}) - \left[R_{rs}(\lambda_{blue}) + \frac{(\lambda_{green} - \lambda_{blue})}{(\lambda_{red} - \lambda_{blue})} * (R_{rs}(\lambda_{red}) - R_{rs}(\lambda_{blue}))\right] \quad (1)$$

where R_{rs} (λblue, λgreen and λred) are spectral bands in the wavelengths closest to 443, 555 and 670 nm respectively, CI is the color index.

$$log_{10}(chlor - a) = a_0 + \Sigma_{i=1}^{4} a_i \left(log_{10}\left(\frac{(R_{rs}(\lambda_{blue})}{(R_{rs}(\lambda_{green})}\right)\right)^i \quad (2)$$

where the numerator, R_{rs} (λblue) is the highest of several input R_{rs} values and coefficients, a_0-a_4, are sensor-specific (0.2424 and -1.2280 for MODIS, and 0.2228 and -0.7768 for VIIRS (OC3), respectively. Chl-a is the output of Chl-a concentration in mg/m^{-3}.

The water color index algorithm is used for Chl-a concentration below 0.15 mg/m^{-3}, while the band rationing algorithm is used for concentrations above 0.2 mg/m^{-3}. Both algorithms are combined for concentrations between these values, using the weighted method (Feldman, 2020a).

In this study, 45 level 2 VIIRS (SNPP) Chl-a concentration products were downloaded from the OceanColor website for the Arabian Gulf region. The data cover all twelve months of 2017. The pixel size of

level 2 data is 1 square km, and temporal resolution is daily. On the other side, 64 seasonal level 3 VIIRS (SNPP) Chl-a concentration products for the Arabian Gulf were ordered and used. The data cover eight years from 2012 to 2019 with one product covering each season (4 products for each year). This means that one product constitutes geophysical mean values of about 30 daily images. So, the level 3 data used in this study refer to more than 2,929 analysed Chl-a daily level 2 products. The spatial resolution of level 3 products is 4 and 9 square km. The 4 km product was used. The reason for choosing the 2017 level 2 products are calibration and verification using KEPA GTPs, while level 3 data were chosen due to spatial and temporal differences and coverage.

3.3. Prediction and validation

Although the Chl-a products of VIIRS - SNPP are modelled using in-situ data (Feldman, 2020b), and many studies have demonstrated the accuracy of these data (Al-naimi et al., 2017; Kahru et al., 2014), the products must be validated locally. The correlation between satellite and near-surface Chl-a concentration may be affected by several local properties, broadly speaking controlled by the geographical and oceanographic conditions (Jensen, 2016). Therefore, GTPs (n = 192) observed by 15 stations covering all Kuwaiti waters were used to build and validate a new empirical local model. Linear regression analysis was used to build the model that reflects the correlation between GTPs and satellite level 2 Chl-a products (OC3). The following matrix was used to compute the regression algorithm:

$$\begin{bmatrix} Chlor-a_1 \\ Chlor-a_2 \\ . \\ . \\ . \\ Chlor-a_n \end{bmatrix} = \begin{bmatrix} \beta_0 + \beta_1 & Raster_1 \\ \beta_0 + \beta_1 & Raster_2 \\ & . \\ & . \\ & . \\ \beta_0 + \beta_1 & Raster_n \end{bmatrix} + \begin{bmatrix} \in_1 \\ \in_2 \\ . \\ . \\ . \\ \in_n \end{bmatrix} \qquad (3)$$

where β_0 and β_1 are population Chl-a intercept and population slope coefficient. $Raster$ is the Chl-a (OC3) product at specific points and ϵ is random error. $Chlor-a$ is the predicted output of Chl-a values.

A window of 3*3 pixels was built around each GTP to extract the satellite data for matching. This technique was used in previous studies (Albanai, 2019; D'Alimonte and Zibordi, 2003). The satellite data that have the standard deviation of more than 3 mg/m^{-3} were omitted from the analysis to improve matching accuracy. The GTPs were divided into two groups: GTPs (n = 113) monitored in three seasons (spring, summer and autumn) were used to find the correlation and build the model, while GTPs (n = 79) observed in winter were used to validate the predicted model (through a seasonal cross-validation process). The correlation was positive where r^2= 0.792 (Fig. 2 and Fig. 3). The credibility of the extracted model was increased by calculating the correlation index (d). The index had previously been proposed by Willmott (Willmott, 1981) for geographical model evaluation. The index can measure predication model error on the 0-1 scale, where 1 indicates perfect correlation, while 0 means no correlation at all. However, due to squared differences, the index is sensitive to outliers. The (d) index can be calculated as follows:

$$\boldsymbol{d = 1 - \frac{\sum_{i=1}^{n}(x_i - y_i)^2}{\sum_{i=1}^{n}\left((|y_i - \bar{x}_i|) + (|X_i + \bar{x}_i|)\right)^2}} \qquad (4)$$

where x_i and y_i are the observation and forecast values, respectively.

The accuracy of the empirical regression model was examined through the root mean square error (RMSE) and the mean absolute error (MAE). These two indices are used to determine the correlation between two variables quantitatively, and were used in several similar studies (Al-Yamani and Naqvi, 2019; Marrari et al., 2006; Zhang et al., 2006). The RMSE and MAE are calculated as follows:

$$RMSE = \pm\sqrt{\frac{1}{n}\sum_{i=1}\left(f_i - f_j\right)^2} \qquad (5)$$

$$MAE = \frac{1}{n}\sum_{i=1}\left|f_i - f_j\right| \qquad (6)$$

where f_i is the value of the derived empirical model, and f_j the value of GTPs.

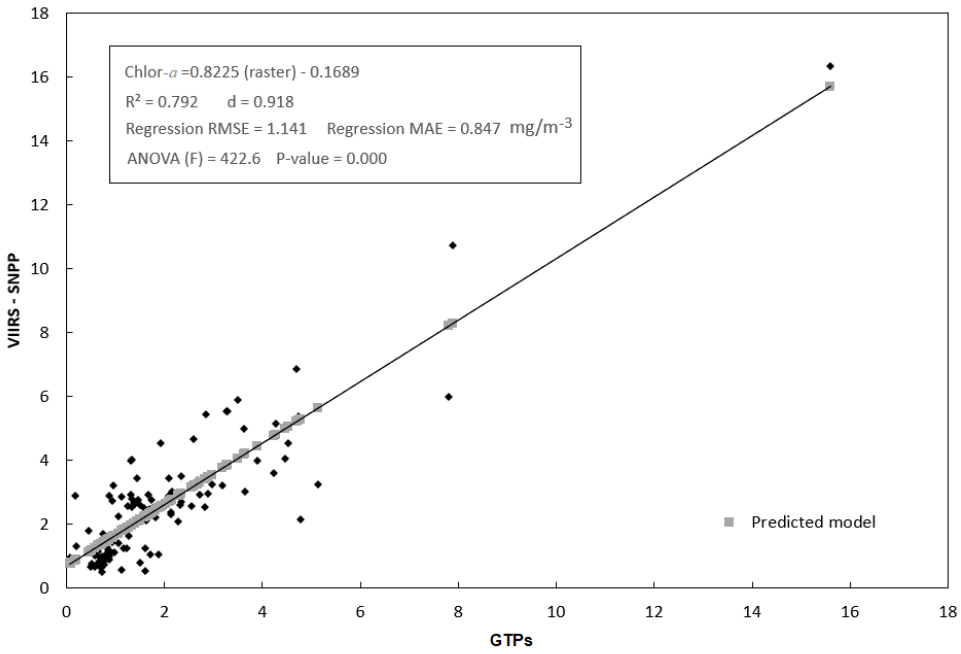

Figure 2. The correlation between GTPs and satellite data of VIIRS – SNPP level 2 products was estimated as positive through regression analysis

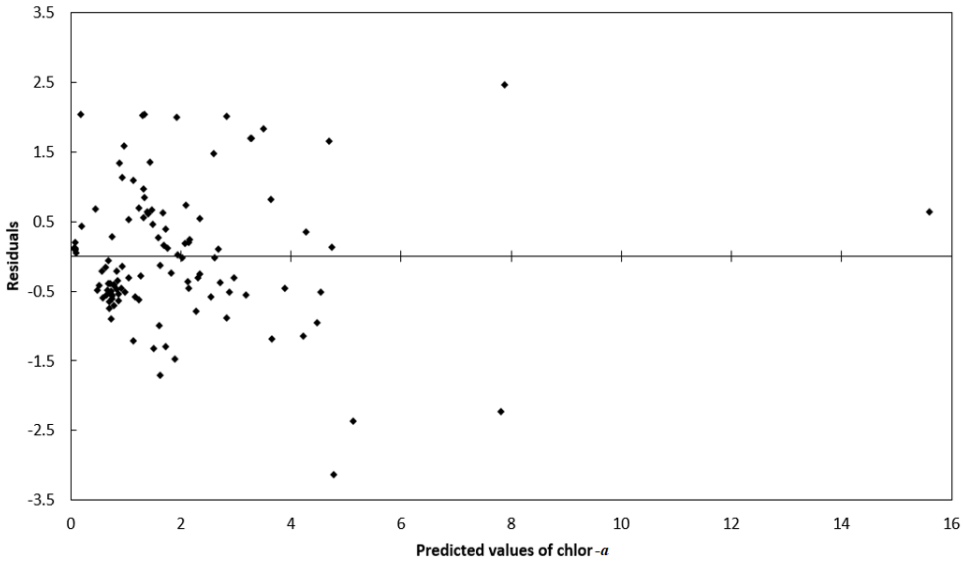

Figure 3. The residual plot shows that the points are randomly dispersed around the horizontal axis, confirming the appropriateness of the linear regression model for the data

3.4. Raster analysis and spatial enchantment

The level 3 Chl-a concentration VIIRS – SNPP products have been geometrically corrected to the WGS 84 coordinate reference system in the BEAM – DIMAP format using the SeaDAS 7.5.3 software. This format can be used in the ArcGIS Pro software for further analysis. Following that, the regression algorithm was applied to seasonal products. The Arabian Gulf data were directly analysed by extracting the spatial mean and standard deviation for each seasonal plate. The spatial mean is the average of all the pixels in the study area, where the standard deviation of the spatial mean describes the deviation of Chl-a concentration values from the average. The seasonal mean values for the Arabian Gulf were used to show how the average changed over the study period. Moreover, the geophysical values of the north-west Arabian Gulf for each plate which covers Kuwaiti territorial waters have been clipped for analyses. The spatial resolution of level 3 product data was 4 square km, which means that the data were limited to mapping large-scale areas, such as Kuwaiti waters (8,000 square km). On the other hand, although the data used have acceptable spatial coverage, they falter in narrow areas, such as the creeks and embayments found in Kuwait's northern marine environment around Bubyan and Warba islands, as well as some parts of the Kuwait Bay. This issue was resolved by extracting the values of each pixel on the North West Arabian Gulf to build an inverse distance weighted (IDW) model. The IDW is a method of estimating an unknown point value from several surrounding known point values. The best results for this model are obtained when the distribution of control points (samples) is of high density and has a wide spatial spread over the study area concerned, in order to simulate all existing spatial differences; otherwise, the results of the model may be affected (Watson and Philip, 1985). The IDW method has higher accuracy in the spatial enhancement of raster model with conditions of high variation coefficient values, strong anisotropy and spatial structure (Chaplot et al., 2006). These conditions were relatively identical to those in the model used. Additionally, Musashi et al. (2018) showed that this model was more accurate than other derivative models. The IDW model was created based on 2,000 extracted values from the north-western Arabian Gulf, and has facilitated maximum spatial resolution increase, as determined by the function in the ArcGIS Pro 2.3 toolbox (spatial analyst – interpolation tools) based on the number of points entered (Fig. 4). The following algorithm was used to calculate the inverse distance weighted (IDW) model:

$$zx_0 = \Sigma_{i=1}^{n} x_i / h_{ij}^{\beta} + \Sigma_{i=1}^{n} 1 / h_{ij}^{\beta} \qquad (7)$$

where *z* (x_0) is the output value, x_i is the value of known control points, *hij* is the separation distance between interpolated value and control point value, *ß* is the weighting power, and *n* is the total number of control points (samples) values.

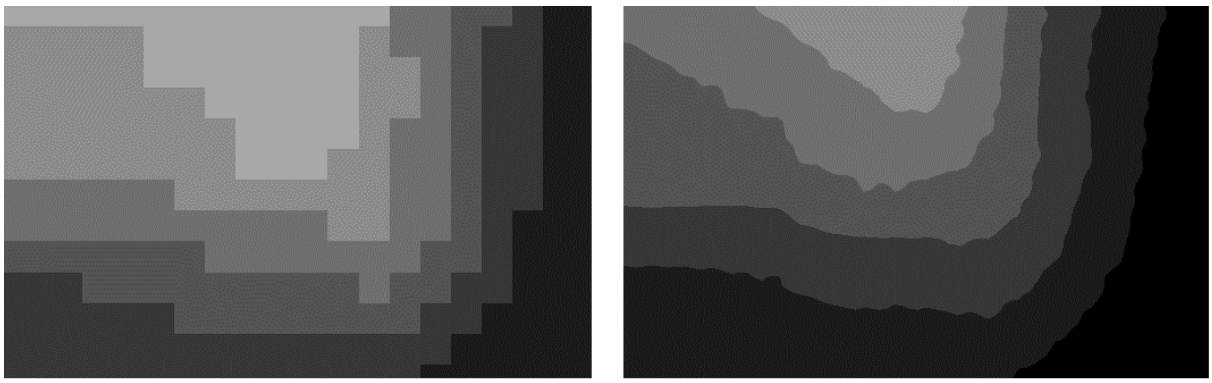

Figure 4. Increasing the spatial resolution by applying the inverse distance weighted (IDW) model to the geophysical values of Chl-a concentration products in the north-west Arabian Gulf

Following that, Kuwaiti waters were divided into north waters, the Kuwait Bay, and south waters (Fig. 5). The division was based on the similarities and differences of marine properties mentioned in the study area description. Mean and SD of each region were computed using zonal statistics. Additionally, Kuwait's territorial waters were divided into three areas based on their depth to show the correlation between near-surface Chl-a and the depth of Kuwaiti waters. The mean value and SD for each class were calculated as well.

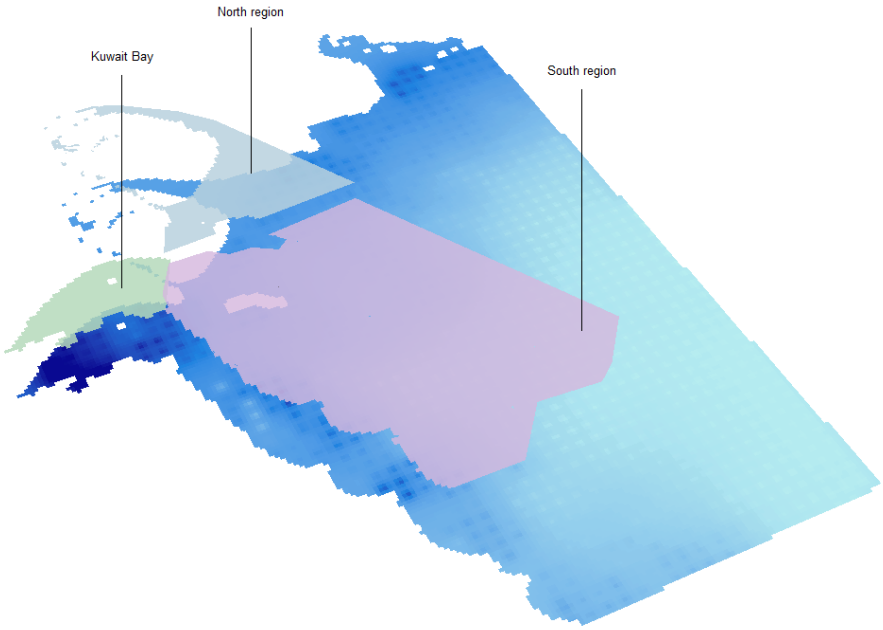

Figure 5. The sub-regions of Kuwaiti waters: the north region, the Kuwait Bay and the south region

Through 57 spatial mean GTPs, the IDW seasonal model was examined using the Mann Whitney test. The Mann Whitney test is a statistical hypothesis test used to compare two populations based on their medians/means. This test can be used when the data do not follow a normal distribution, in addition to other non-parametric testing conditions (Coleman, 2015), noticeable in Chl-a concentration histograms. The following formulae were used to conduct the Mann Whitney test:

$$U = min\ (U_1, U_2)$$

where:

$$U_1 = n_1 n_2 + \frac{n_1(n_1+1)}{2} - R_1$$

$$U_2 = n_1 n_2 + \frac{n_2(n_2+1)}{2} - R_2 \qquad (8)$$

where η_1 and η_2 are sample sizes, R1 and R2 the sums of observations rank from sample 1 and 2 populations, respectively.

Fig. 6. shows the methodology summary, from downloading the data to the spatial analysis through pre-processing and GTPs.

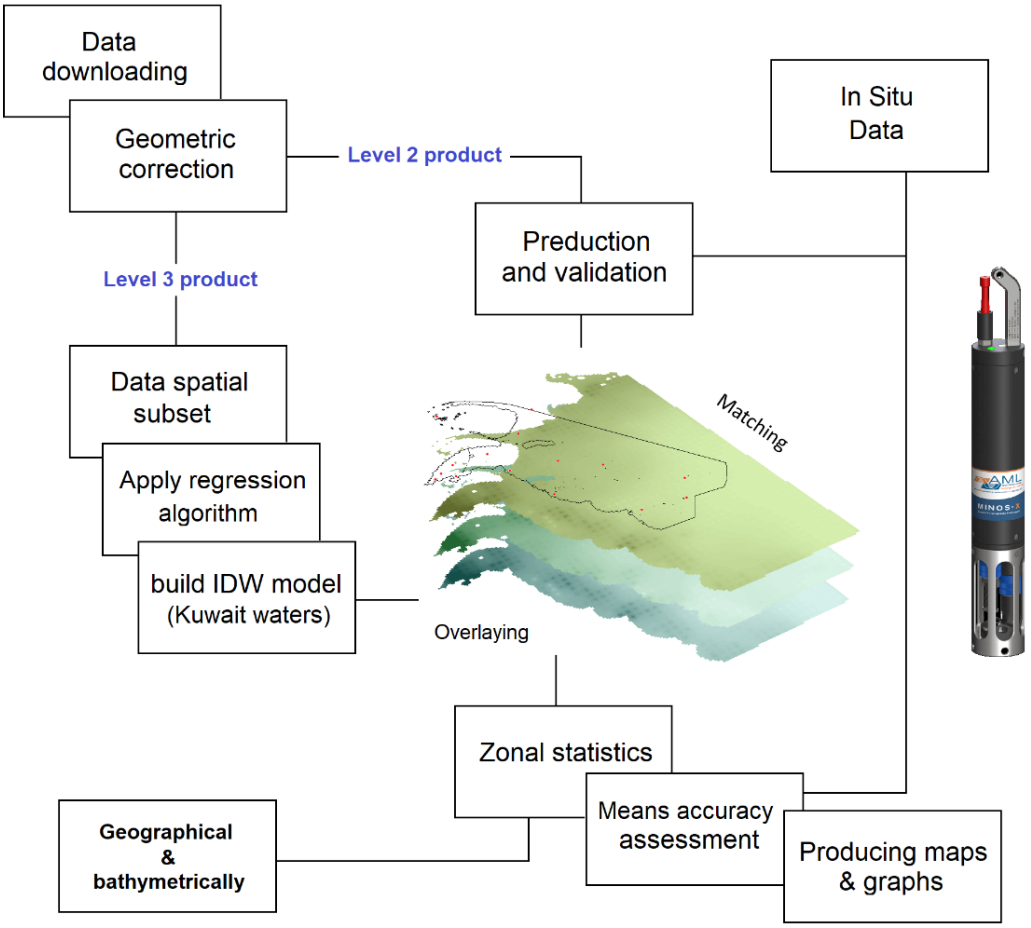

Figure 6. Summary of the methodology used. Data collection, pre-processing, analysis and assessment steps

4. RESULTS AND DISCUSSION

4.1. Accuracy assessment

The validation results of the empirical level 2 Chl-a concentration model derived from SNPP – VIIRS spectrometer using GTPs (number = 79) monitored in the winter of 2017 and taken by 15 marine buoys showed a significant correlation. The statistical indices confirmed the strong correlation, where the overall RMSE and MAE were = ± 0.841 and 0.638 mg/m^{-3}, respectively. Thus, the empirical model has improved the accuracy by 0.329 and 0.256 mg/m^{-3} where the RMSE and MAE were = ± 1.17 and 0.841 mg/m^{-3} prior to the application of the regression algorithm. Additionally, a wider perspective was obtained by dividing GTPs into two different ranks according to their geographical location and concentration levels. Geographically, they were divided into two regions, with the Kuwait Bay and the northern waters being considered a single region; these showed RMSE and MAE of ± 1.11 and 0.89 mg/m^{-3}. The northern waters were considered together with the Kuwait Bay due to their relative lack of GTPs. By contrast, the southern region showed an RMSE and MAE of ± 0.53 and 0.44 mg/m^{-3} (Fig. 7). The GTPs were also divided into two classes (< 2 and > 2). Lower concentration values were more accurate (RMSE = ± 0.552 and MAE = ± 0.468 mg/m^{-3}) than the higher concentration values (RMSE = ± 1.09 and MAE = ± 0.84 mg/m^{-3}) (Fig. 8).

The regression algorithm was applied to the IDW model derived from level 3 Chl-a concentration data. The correlation between the seasonal averages of the IDW model and the seasonal averages of GTPs (n = 57)

recorded by 15 marine buoys in 2017 was tested using the Mann Whitney test, where the null hypothesis was rejected (sig = 0.948, $p < 0.01$ - 99% confidence). Overall, the empirical model established lower average Chl-a concentration values in the study period and area, meaning that primary Chl-a products of SNPP -VIIRS had been overestimated (Table. 1 and Fig. 9).

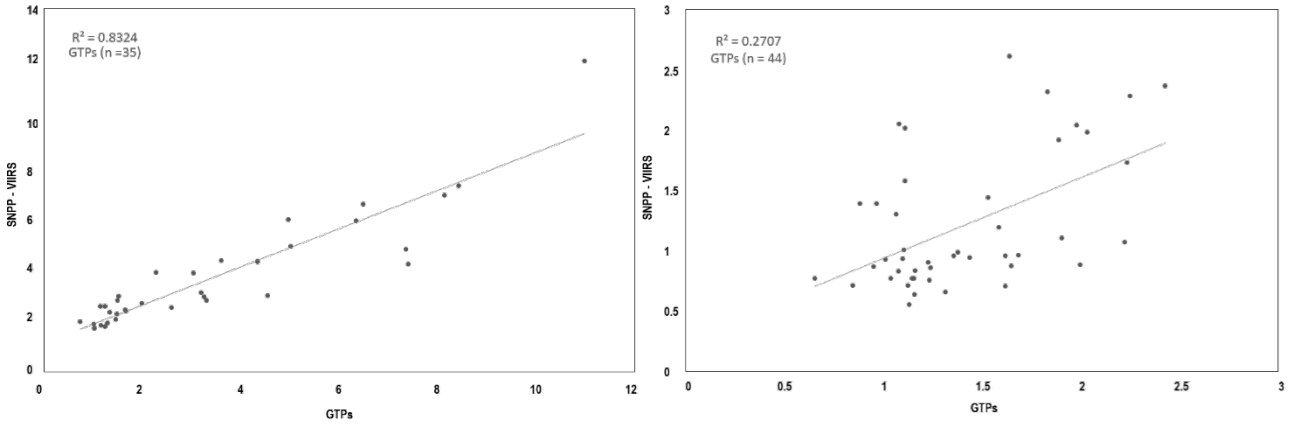

Figure 7. The correlation between GTPs (n = 35) and the empirical model in the Kuwait Bay and the northern waters (a), and the correlation between GTPs (n = 44) and the empirical model in the southern waters (b)

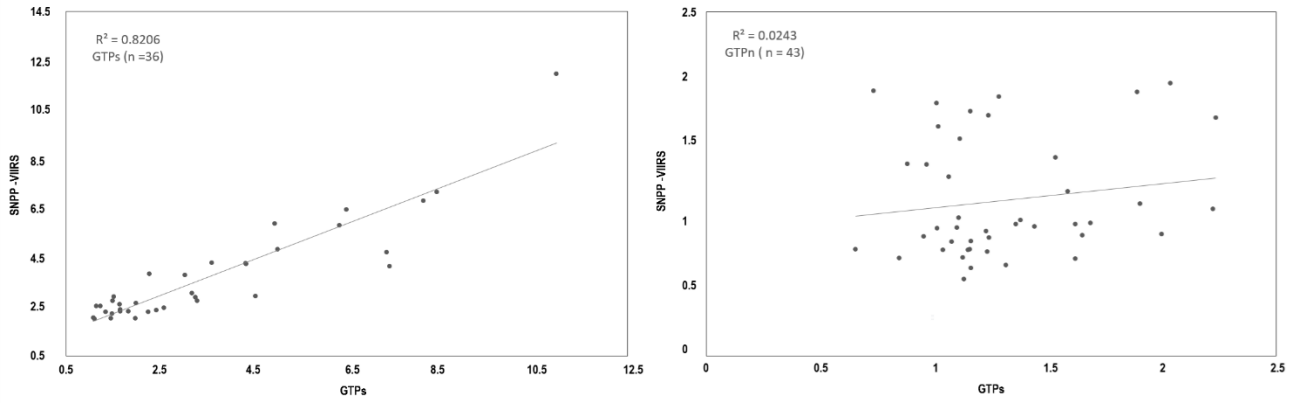

Figure 8. The correlation between GTPs (n = 43) and the empirical model with concentration values lower than 2 mg/m-3 (a), and the correlation between GTPs (n = 36) and the empirical model with concentration values above 2 mg/m-3 (b)

	By value		By location		Overall
	< 2	> 2	Kuwait Bay & North	South region	
RMSE (±)	0.552	1.09	1.113	0.533	0.841
MAE (±)	0.468	0.84	0.89	0.437	0.639

Table 1. Accuracy assessment by value, location and overall in Kuwaiti waters

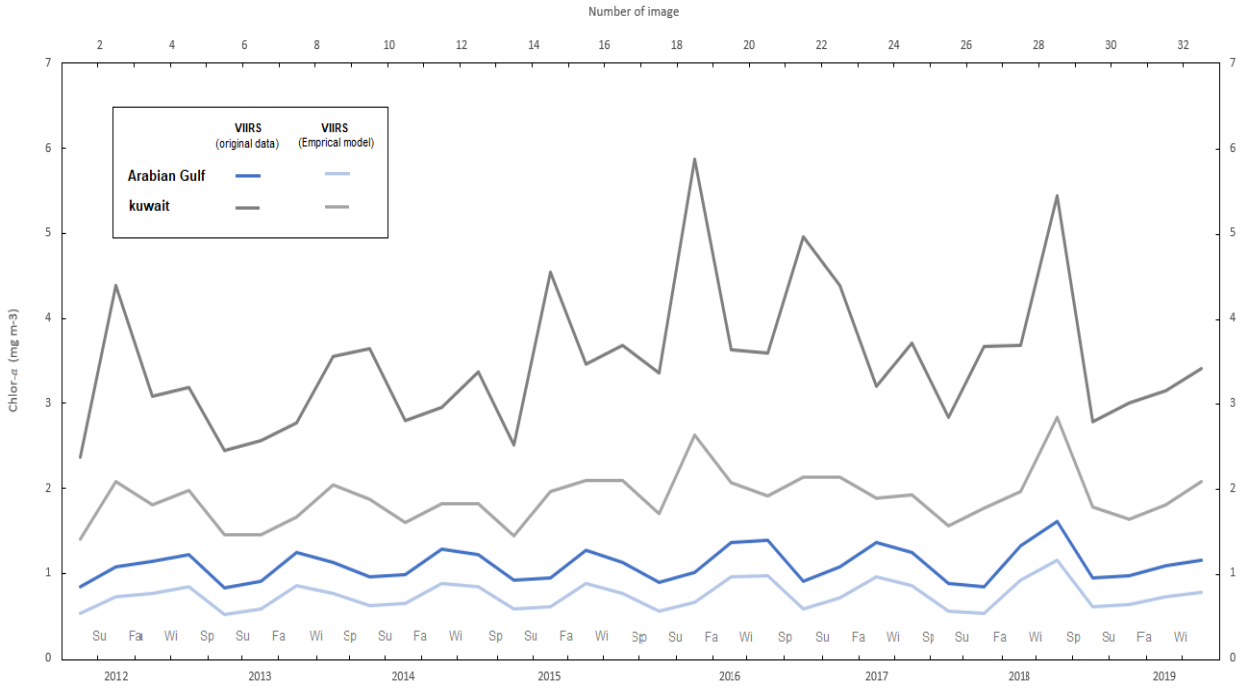

Figure 9. Chl-a average fluctuations in 2012-2019 using the empirical model data from this study and VIIRS – SNPP original product data for both Kuwait and the Arabian Gulf

Empirical model validation results were more accurate for low-concentration water monitoring, and their accuracy decreased in high-concentration waters. This pattern is inevitably affected by depth. Accordingly, the accuracy was measured geographically where the average depth is known. The results confirmed that the accuracy improves in deep water (southern waters of Kuwait), and decreases in shallow and turbid waters (Kuwait Bay and northern waters) (Table 2). When the extracted Chl-a concentration was reviewed using different equations and the NASA satellite sensors for other seas and different bays around the world, with different GTP numbers (30-114), the accuracy in literature varied from 0.18 to 0.64 mg/m^{-3} (Brewin et al., 2013; Hattab et al., 2013; Kahru et al., 2014; Shang et al., 2014). The accuracy was estimated at 0.23 mg/m^{-3} in the middle of the Arabian Gulf using 29 GTPs (Al-naimi et al., 2017), and thus the accuracy of the empirical model developed in this study falls within a reasonable range, especially in a complex environment such as the north-western Arabian Gulf.

Despite the advantages of remote sensing data and solutions, this method does have some limitations. One of these limitations is that the accuracy of the obtained Chl-a concentration results is affected by water depth and high turbidity (Reilly et al., 2000). This is perhaps one of the most important characteristics of the Arabian Gulf, especially of its north-western region (Alyamani et al., 2004). Therefore, developing a new and validated local model is essential (Alyamani et al., 2004). However, the northern part of Kuwaiti waters is considered one of those areas where Chl-a models rarely obtain sensor spatial resolution and coverage data, among other things due to weather factors, such as dust bands (Nezlin et al., 2010; Zhao and Ghedira, 2014). Accordingly, the developed spatial interpolation model for this region does have some limitations, especially with insufficient GTPs available to calibrate the results.

	South region		North region & Kuwait Bay	
	mean	SD	mean	SD
Spring	4.14	7.39	5.45	7.19
Summer	2.65	7.37	6.23	7.25
Fall	5.57	7.37	6.46	7.32
Winter	2.69	7.33	6.13	7.32
Overall	3.76	7.36	6.07	7.27

Table 2. The turbidity seasonal averages and standard deviation (NTU) obtained from KEPA buoys in 2017. The Kuwait Bay and the northern waters are characterized by higher turbidity than the southern waters throughout the year.

4.2. Spatial-temporal variation

Based on the sub-division of the Arabian Gulf (Polikarpov et al., 2019) (Fig. 1), and given our knowledge of water circulation and Gulf bathymetry (Polikarpov et al., 2019), the analysis of seasonal averages in 2012-2019 using the SNPP - VIIRS spectrometer showed that the coastal areas have higher Chl-a concentrations compared to those in the open waters. As for coasts, the Iranian eastern coast has a lower concentration than western coasts. However, the northern Shatt al-Arab coastal zone had the highest concentration of Chl-a in winter and late autumn, especially its western parts, where the Kuwaiti waters are located (Fig. 10 and Fig. 11). In this area, the Kuwait Bay has the highest concentration of Chl-a as, in the southern waters, the deep-water characteristics begin to become clear. The northern waters also have high Chl-a concentration compared to the southern waters, (Fig. 12 and Fig. 13). The physical, topographical and anthropogenic factors contribute to the high level of Chl-a in the north-western zone: low depths contribute to the influx of nutrients from the deep rich layers (Polikarpov et al., 2019), the discharge of the rivers in the northern Arabian Gulf, the general water circulation in the Gulf that carries nutrients to the north-western coasts of the Arabian Gulf (Polikarpov et al., 2019), and the human stresses on the coastal areas (Polikarpov et al., 2019). However, they point out that an overestimation by remote sensing instruments can happen in this area due to high turbidity (see Table 2) and bottom reflection.

As for seasonal fluctuations, Chl-a concentration in the Arabian Gulf in 2012-2019 was at its lowest in spring, with the quarterly average of 0.57 mg/m^{-3}. The concentration increases in summer with the 0.64 mg/m^{-3} average. The concentration continues to increase in early autumn, with the average hitting 0.87 mg/m^{-3}, and remaining fairly steady in winter. In this season, the high concentration is noticeable in the north-western region, and on the western coasts, as well as at the entrance to the Arabian Gulf in the Strait of Hormuz, where the concentration increases significantly until it reaches around 6 mg/m^{-3} (Table 3). The sub-regions of Kuwait's waters follow a seasonal pattern comparable to the general seasonal cycle in the Arabian Gulf waters. The seasonal peak is reached in autumn and winter, while the concentration reaches a low in the summer. However, the annual average concentration of Chl-a in the Kuwait Bay increases significantly, with 1.86 mg/m^{-3} in the south, and 0.57 mg/m^{-3} in the north. Fig. 14 illustrates seasonal differences, while Table 4 looks at both the averages and the standard deviation variation. The drop in Chl-a concentrations in autumn is often due to nutrients being depleted by the phytoplankton bloom in winter (Al-naimi et al., 2017). Nezlin et al. (2007) clearly show that the seasonal cycle of Chl-a concentration in tropical and subtropical oceans is typical because phytoplankton growth is affected by nutrient depletion resulting from pycnocline build-up, in addition to the effects of thermal stratification in the water column, which limits vertical mixing and nutrients float to the surface (Doney, 2006). This study result is consistent with other seasonal fluctuation studies (Al-naimi et al., 2017; Moradi and Kabiri, 2015; Nezlin et al., 2007).

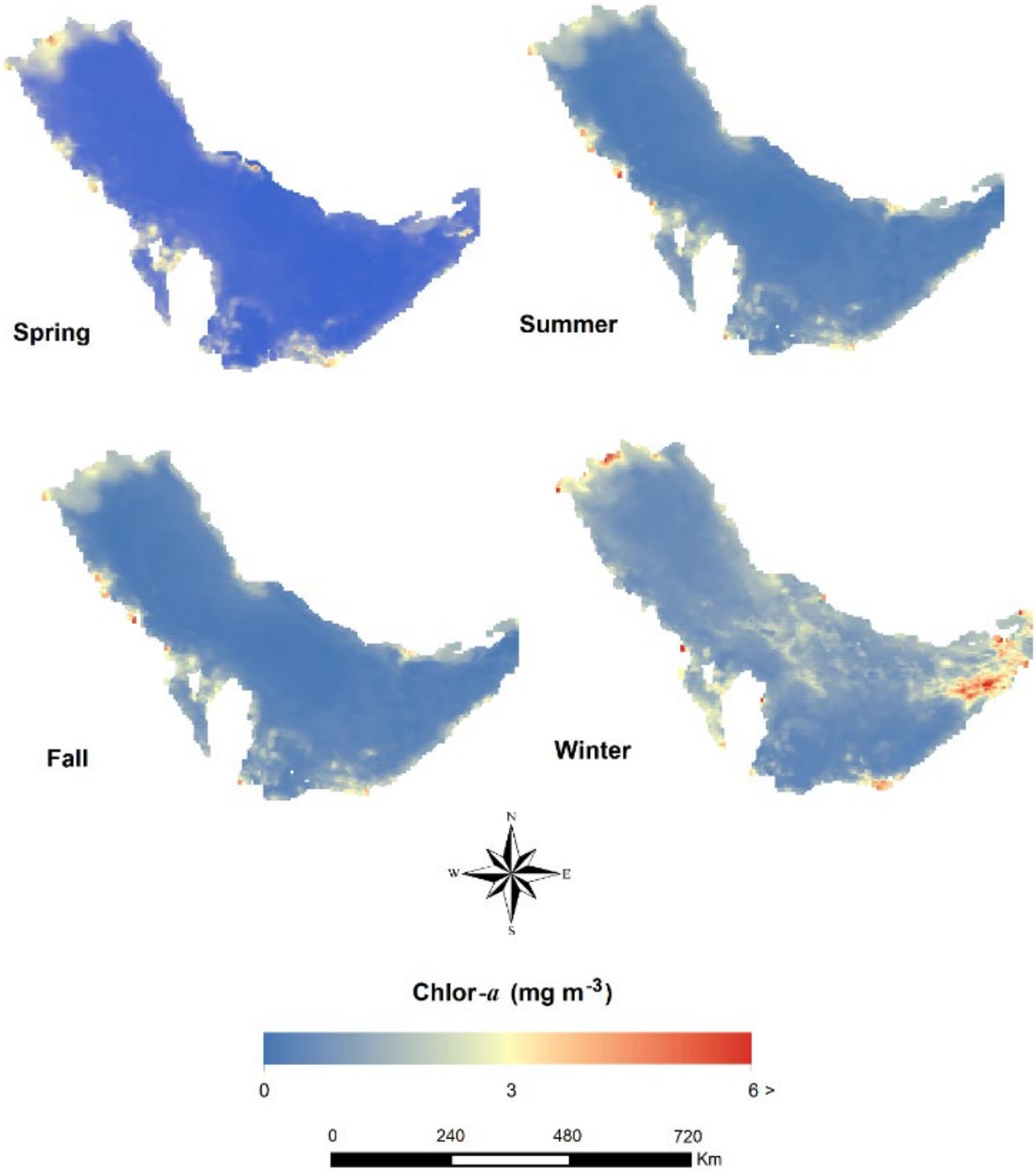

Figure 10. The spatial distribution of Chl-a concentration seasonal averages in the Arabian Gulf in 2012-2019. Chl-a concentration increases in winter in the Strait of Hormuz and in the northern waters of the Arabian Gulf

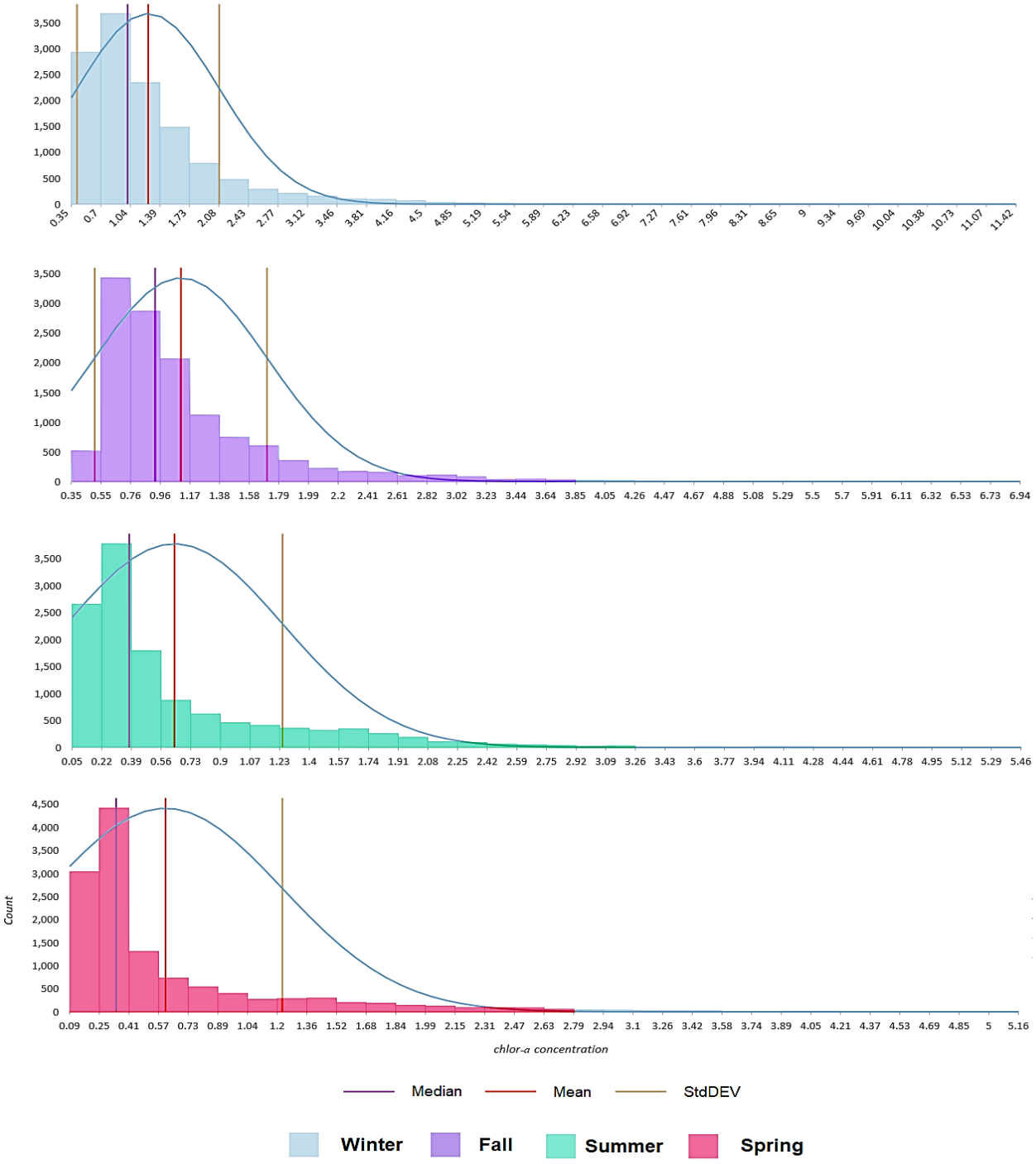

Figure 11. The statistical distribution of Chl-a concentration seasonal averages in the Arabian Gulf in 2012-2019. Chl-a concentration fluctuations increase in summer and spring, and are more gradual in winter and autumn.

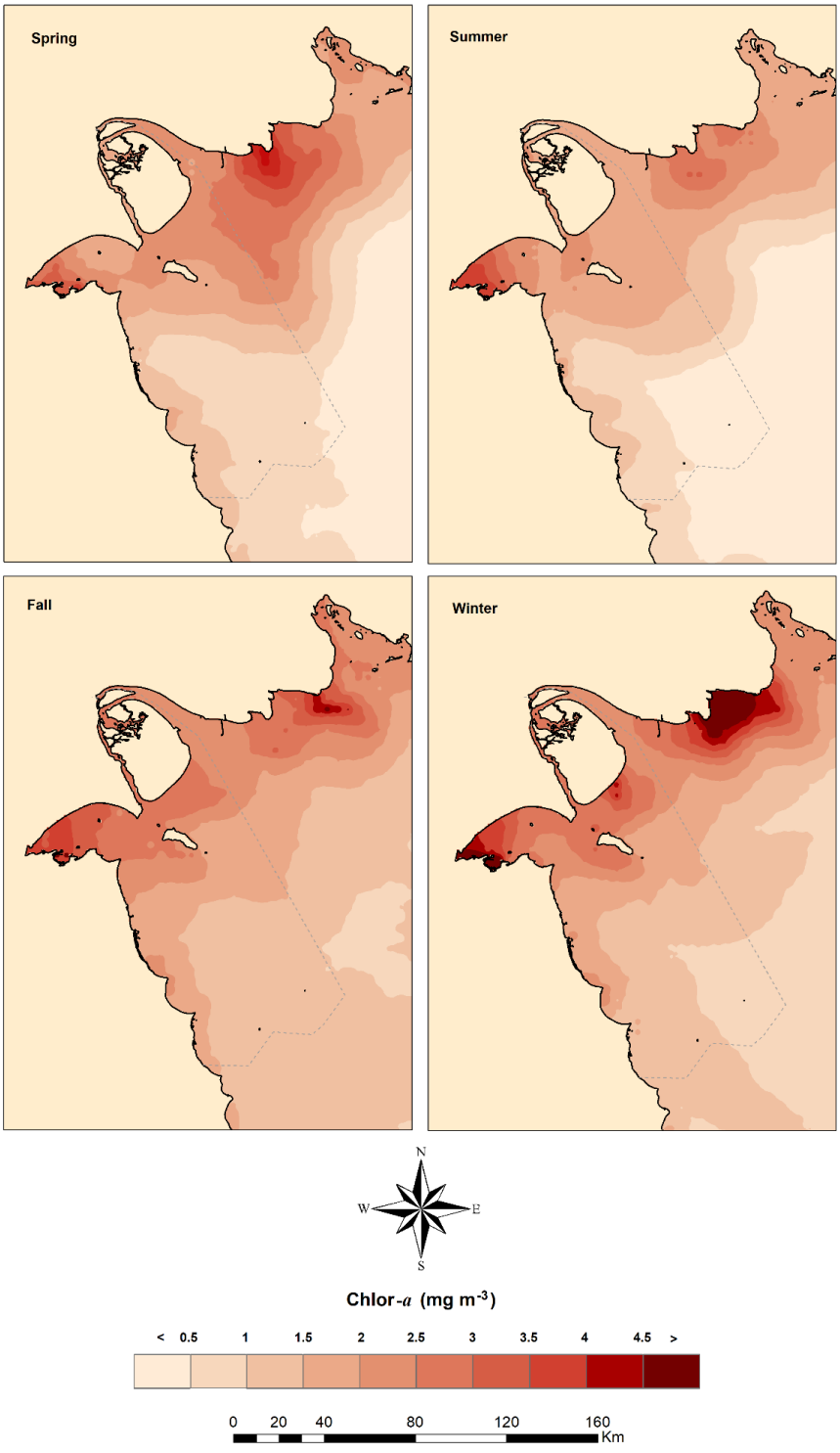

Figure 12. The spatial distribution of Chl-a concentration seasonal averages in Kuwaiti waters and the north-western Arabian Gulf in 2012-2019. Chl-a concentration increases in winter in the Kuwait Bay and the northern waters of the Arabian Gulf.

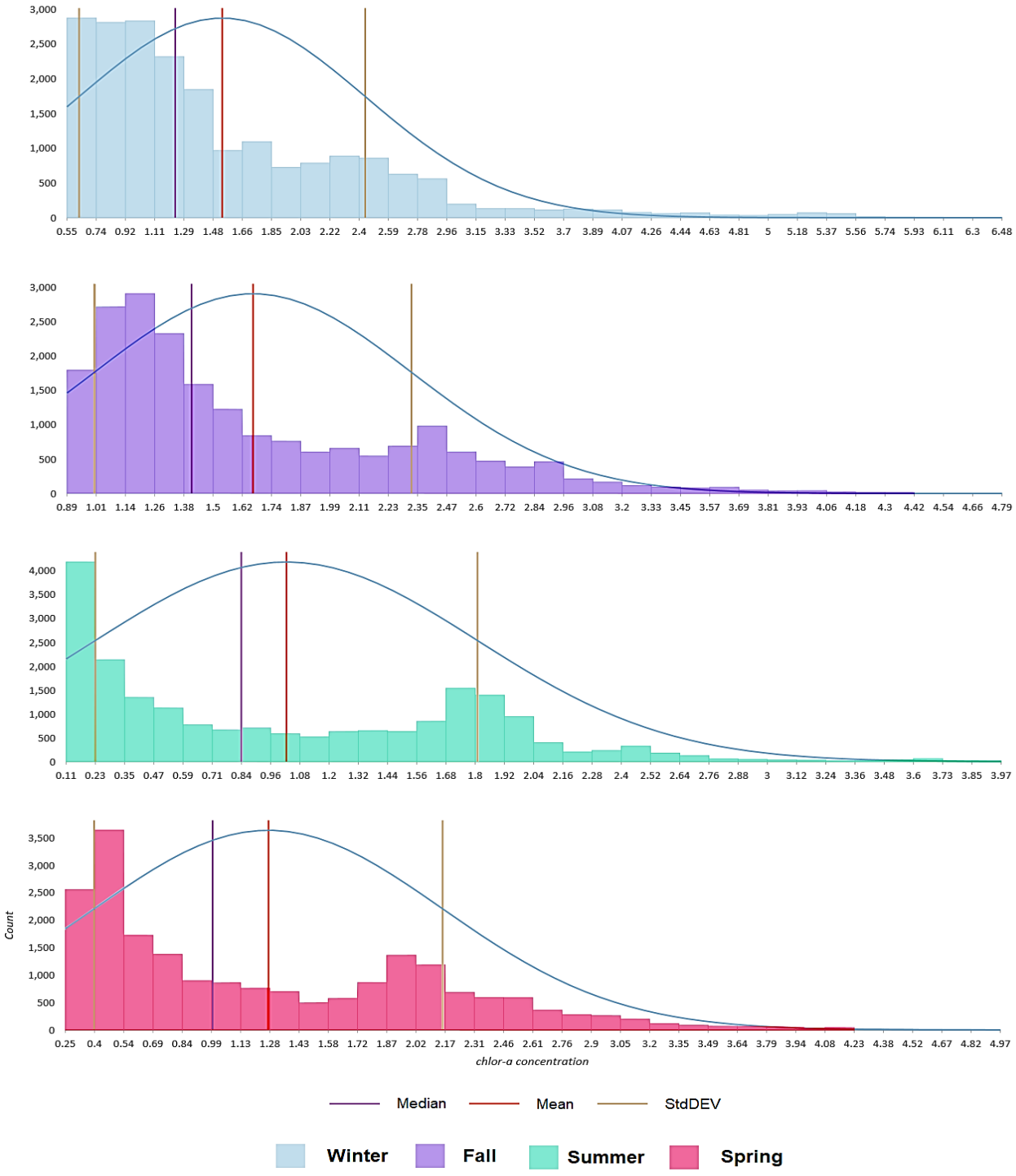

Figure 13. The statistical distribution of Chl-a concentration seasonal averages in Kuwaiti waters and the north-western Arabian Gulf in 2012-2019. The peak of the seasonal curves can be seen at low concentrations. A clear second smaller peak of Chl-a concentration can be observed at 1.8 - 2 mg/m^{-3} in summer and spring.

	Kuwait		Arabian Gulf	
	mean	SD	mean	SD
Spring	1.88	0.38	0.57	0.38
Summer	1.81	0.43	0.64	0.5
Fall	2.41	0.35	0.87	0.47
Winter	2.38	0.56	0.87	0.48
Overall	2.12	0.43	0.74	0.46

Table 3. Seasonal means and standard deviations for the Arabian Gulf and Kuwaiti territorial waters

	Kuwait Bay		South region		North region	
	mean	SD	mean	SD	mean	SD
Spring	2.3	0.48	1.11	0.48	2.22	0.18
Summer	2.64	0.65	0.93	0.52	1.86	0.12
Fall	3.21	0.38	1.55	0.37	2.47	0.31
Winter	3.21	0.78	1.39	0.45	2.54	0.44
Overall	2.84	0.57	1.24	0.46	2.27	0.26

Table 4. Seasonal means and standard deviation for the sub-regions of Kuwaiti territorial waters in 2012-2019

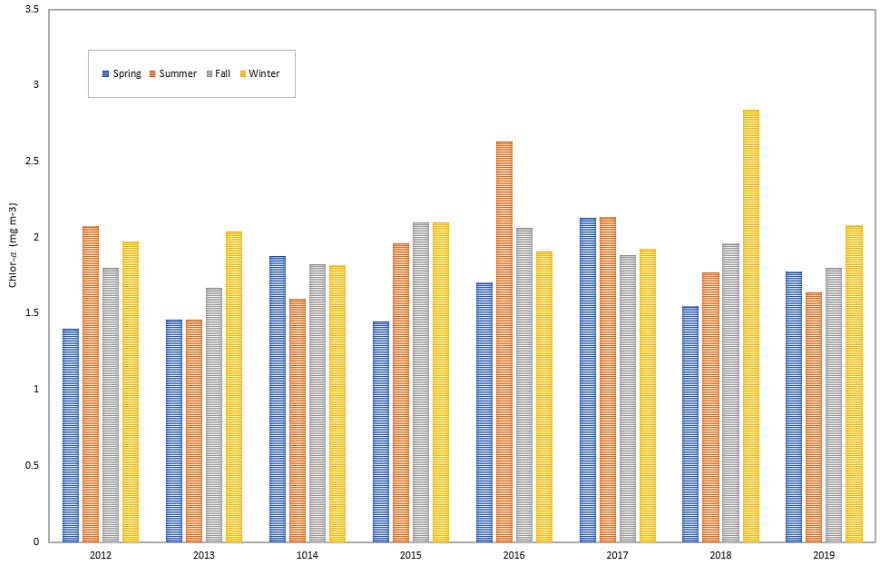

Figure 14. Seasonal averages for Kuwaiti territorial waters in 2012-2019. The seasonal pattern of Chl-a concentration appears to be erratic in Kuwaiti waters.

The Chl-a concentration trend in the Arabian Gulf and Kuwaiti waters in 2012-2019 shows that the average concentration fluctuates in semi-regular seasonal cycles, mostly increasing in winter and late autumn. However, the Chl-a concentration average fluctuated between approximately 0.5 and 1 mg/m^{-3} in the study period, 2012-2019. The highest average concentration was recorded in the winter of 2018, when it exceeded 1 mg/m^{-3} (Fig. 15). Chl-a concentration in Kuwaiti waters shows that the seasonal cycles are less regular and more severe than those in the Gulf as a whole. Kuwaiti waters are situated in the Shatt al-Arab region, which has a higher concentration overall, and a more complex cycle affected by the complex river-sea system. However,

the highest peak was observed in the winter of 2018 and autumn of 2019. The results indicate that the average Chl-a concentration in Kuwaiti waters is increasing (Fig. 16). Fig. 17 shows the seasonal moving average of Chl-a concentrations in sub-regions of Kuwaiti waters in 2012-2019.

Kuwaiti waters are characterized by quarterly concentration fluctuations similar to those in the Gulf as a whole. The recorded high average concentrations in the north-western region of the Arabian Gulf, and especially in the Kuwait Bay, where the values are significantly higher than in the northern and southern regions, are consistent with the study of spatial fluctuations in Kuwait's Chl-a concentration by Alyamani et al. (2004). Additionally, the long-term results showed regular seasonal fluctuations at Arabian Gulf level, with peaks in certain years, as well as less regular fluctuations in Kuwaiti waters, where remarkable leaps were seen, especially in the Kuwait Bay.

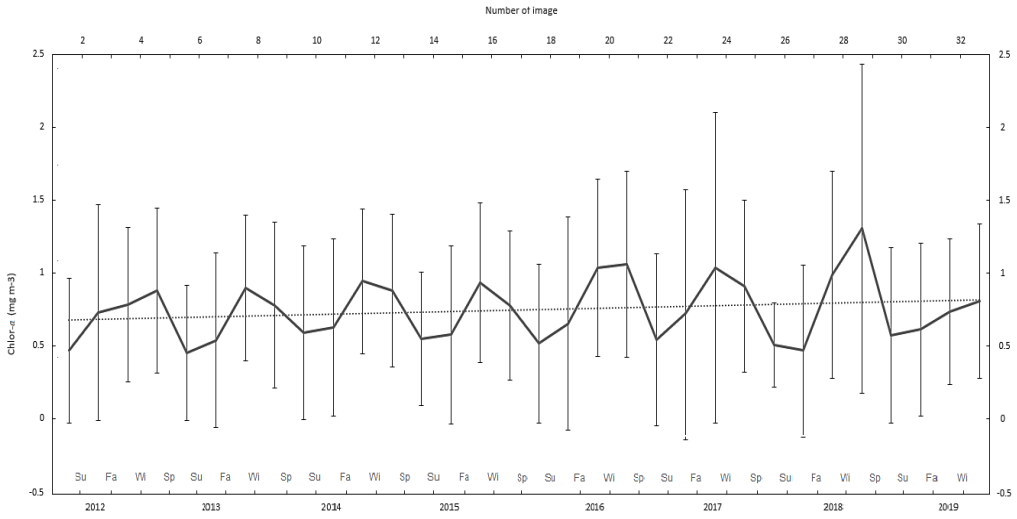

Figure 15. The seasonal moving average trend and pattern of Chl-a concentration in the Arabian Gulf in 2012-2019. A semi-regular cycle can be observed in the study period.

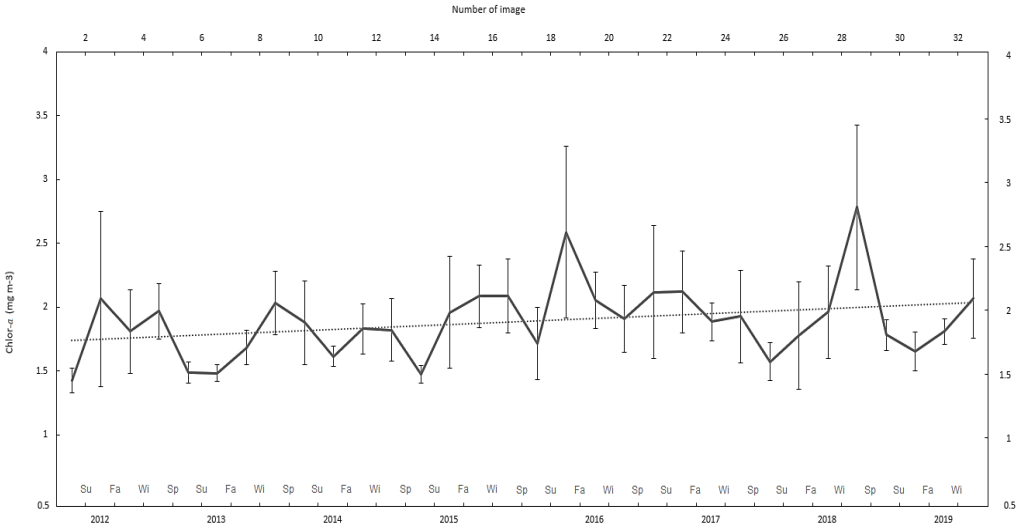

Figure 16. The seasonal moving average of Chl-a concentration in Kuwait's territorial waters in 2012- 2019. Two peaks can be observed in 2016 and 2018.

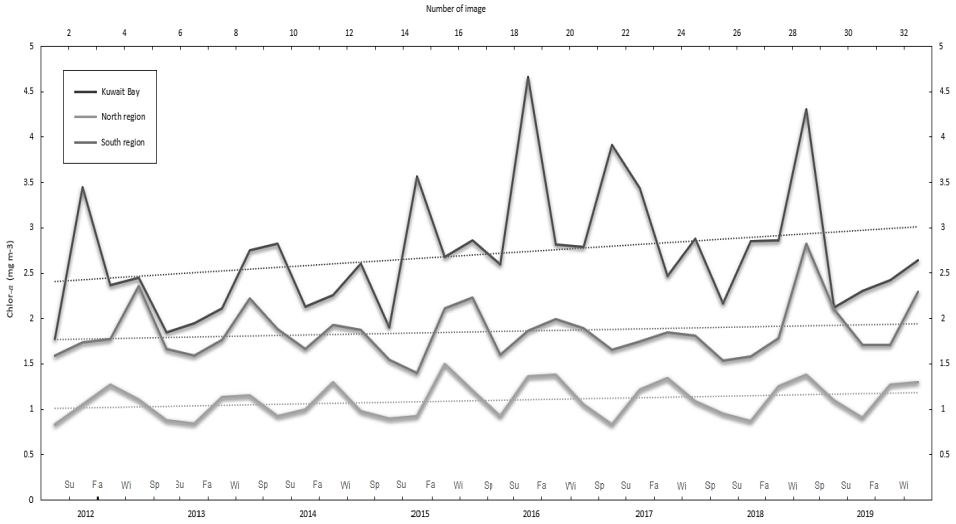

Figure 17. The seasonal moving average of Chl-a concentration in sub-regions of Kuwaiti waters in 2012-2019. The pattern in the Kuwait Bay is more extreme than in the northern and southern waters.

4.3. Chl-a vs. bathymetry

The spatial distribution of Chl-a concentration derived from the empirical model of SNPP – VIIRS level 3 data was studied over three bathymetric classes extracted and analysed by the spatial interpolation model derived from depth GTPs in Kuwaiti waters. The results confirmed that Chl-a concentration is affected by depth, with mean values decreasing with increasing depth. At lower depths (less than 10 meters), the average Chl-a concentration over an eight-year period (2012-2019) was 2.34 mg/m^{-3}. However, the concentration decreases gradually to 1.5 mg/m^{-3} in the depth range of 10-20 meters, and continues to drop until it reaches 0.88 mg/m^{-3} at 20 meters and below. The Chl-a concentration level decreases steadily as depth increases at 10-meter intervals. The standard deviation decreases by about 0.2, with an increase for every ten meters in depth. This correlation applies to all seasons, with similar degrees of decline with increasing depth (Table 5).

Although many studies have indicated that the concentration of nutrients increases until the depth of 1,000 meters in seas throughout the world (Hayase and Shinozuka, 1995; Sunda, 2012), and the mixing process can lift the nutrients from the rich near-bottom to the near-surface layer (Wirasatriya et al., 2018). The limited upwelling process in the Arabian Gulf causes limited nutrient concentration offshore and in the northern open waters of the Arabian Gulf (Johns et al., 2003). This may explain the lower Chl-a concentration in Kuwait's southern waters. By contrast, many sources feed the submerged northern estuarine flat where the Kuwait Bay is situated. The standard deviation of the Chl-a concentration increases slowly with decreasing depth; this suggests that Chl-a concentration is more homogenous in deeper areas, such as Kuwait's southern waters, than in the shallow areas such as the Kuwait Bay, which is a shallow semi-enclosed water, with river freshwater discharge bringing the nutrients from the land. Further anthropogenic stresses and the presence of sewage in the waters of the Bay (Al-Yamani and Naqvi, 2019) may be other reasons behind higher chlorophyll-a concentration and its relatively wide spatial variation. Fig. 18 is a 3D bathymetric model of near-surface Chl-a concentration, which clearly shows the spatial correlation between depth and Chl-a concentration in the north-western Arabian Gulf (Kuwait's waters). The submerged northern estuarine flat has a higher average seasonal concentration compared to other Kuwaiti waters.

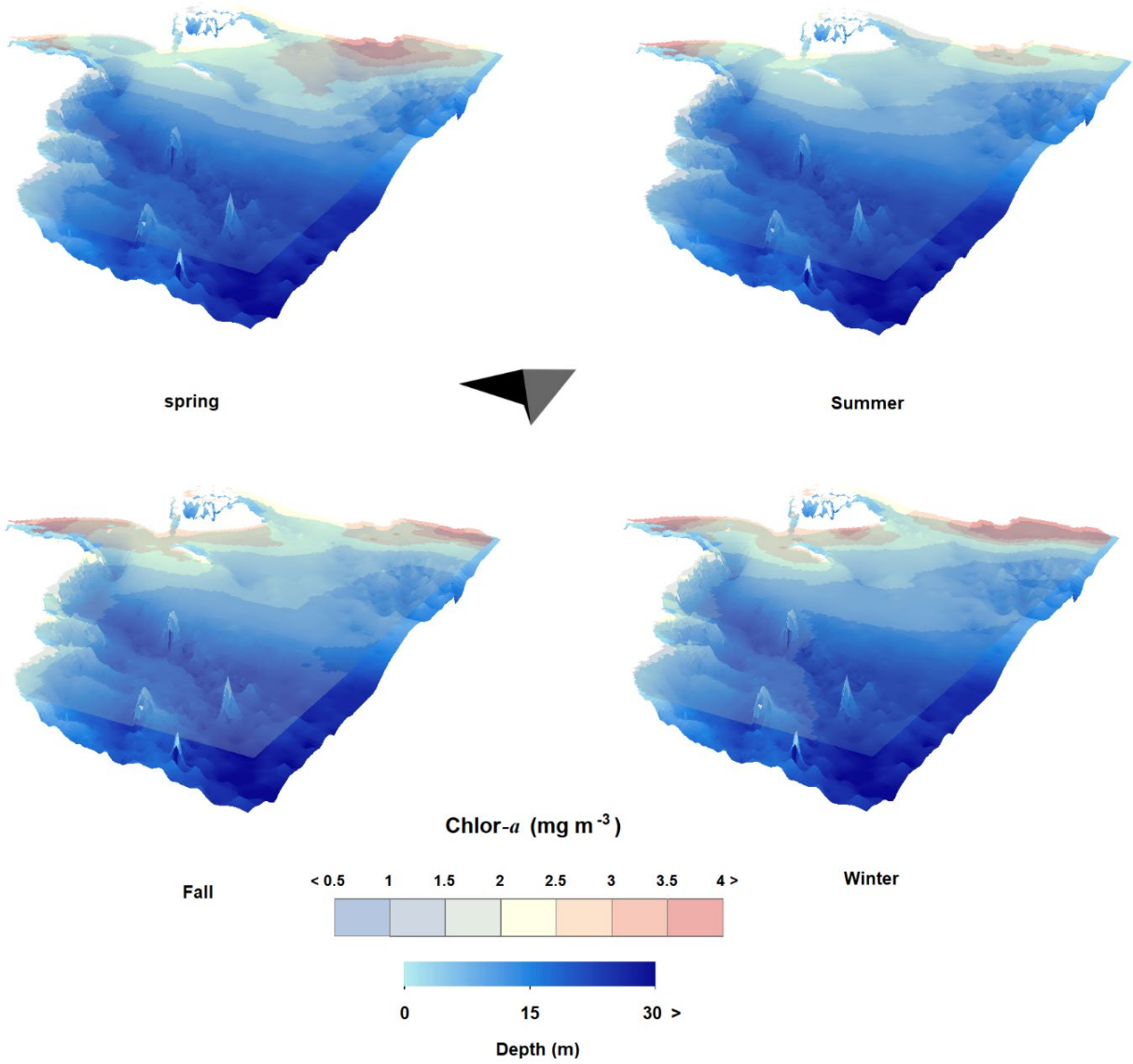

Figure 18. 3D models show the seasonal averages of Chl-a concentration in 2012-2019 in the north-eastern Arabian Gulf bathymetry (Kuwaiti waters). The concentration increases as depth decreases (e.g. in the northern part).

	< 10		10 to 20		> 20	
	mean	SD	mean	SD	mean	SD
Spring	2.32	0.65	1.61	0.66	0.7	0.25
Summer	1.97	0.52	1.2	0.5	0.46	0.3
Fall	2.44	0.59	1.65	0.41	1.29	0.24
Winter	2.64	0.98	1.53	0.43	1.05	0.27
Overall	2.34	0.69	1.5	0.5	0.88	0.27

Table 5. Seasonal Chl-a concentration decreases as water depth increases. Three depth ranges show fluctuating concentration values by averages and standard deviation (data 2012 – 2019).

5. CONCLUSION

The subject of this study is the seasonal spatial and temporal distribution of near-surface Chl-a concentration in the Arabian Gulf and Kuwaiti waters in 2012-2019, explained using SNPP – VIIRS spectrometer data. The study included the use of a new empirical model based on GTPs observed in 2017 in the Arabian Gulf, specifically in the north-west, where Kuwaiti waters are located. Additionally, the relationship between Chl-a concentration and the depth of Kuwaiti waters was studied, where the spatial resolution of the model was improved to clearly show the spatial dimension in this specific area. The results showed that Chl-a concentration is higher near the coasts and in the north-western region of the Arabian Gulf (Kuwaiti waters), which area was spatially enhanced, as well as that Chl-a concentration increases in the Kuwait Bay, decreasing gradually towards the south. Seasonally, Chl-a concentration has a cycle that peaks in winter and early autumn in both Kuwaiti waters and the wider Arabian Gulf. However, the concentration averages trend was more stable in the Arabian Gulf compared to Kuwaiti waters in the study period. Additionally, the Chl-a concentration was observed to decrease at a stable rate as depth increases. The empirical model accuracy was tested through GTPs, and showed an overall RMSE and MAE of 0.841 and 0.638 mg/m^{-3}, respectively. Remote sensing techniques provide a valuable insight into the marine environment, including measuring Chl-a concentration and phytoplankton density in seas and oceans by spatial modelling. The improved experimental model (equation) presented in this study could be used in further research from this study area to monitor future Chl-a concentrations.

CONFLICT OF INTEREST

Author declares that he has no conflict of Interest.

REFERENCES

Albanai, J., 2021. Seawater quality atlas of the state of Kuwait, 1st ed. Center For Research and Studies on Kuwait.

Albanai, J.A., 2022. Accuracy assessment for Landsat 8 thermal bands in measuring sea surface temperature over Kuwait and North West Arabian Gulf. Kuwait Journal of Science 49. Available at: https://doi.org/10.48129/kjs.v49i1.9549

Albanai, J.A., 2021a. Mapping Kuwait bathymetry using passive multispectral remote sensing. Kuwait Journal of Science 48, 1–10. Available at: https://doi.org/10.48129/kjs.v48i4.8978

Albanai, J.A., 2021b. Trend and dynamic of chlorophyll-a concentration over the Arabian Gulf A long-term study using MODIS data (2004 – 2019). Journal of Engineering Researsch 10. Available at: https://doi.org/doi.org/10.36909/jer.12213

Albanai, J.A., 2021c. Coastal Atlas of The State of Kuwait: Geomorphology from Space and Atmosphere. Kuwait Foundation For The Advancement Of Science, Kuwait.

Albanai, J.A., 2021d. Spatial Distribution of Kuwait Coastal Geomorphological Features using Remote Sensing Methods and GIS Solutions. Journal of Social Sciences 49. Available at: https://doi.org/10.34120/0080-049-003-14

Albanai, J.A., 2020. Sea level rise projections for Failaka island in the state of Kuwait. Transactions on Maritime Science 9, 236–247. Available at: https://doi.org/10.7225/toms.v09.n02.008

Albanai, J.A., 2019. A GIS Science Simulation for the Expected Sea Level Rise Scenarios on Failka Island in The State of Kuwait, 1st ed. Center For Research and Studies on Kuwait, Kuwait.

Albanai, J.A., Karam, Q., Ali, M., Annabi-Trabelsi, N., 2022a. Physicochemical factors affecting chlorophyll-a concentrations in the north-western Arabian Gulf and Kuwait's territorial waters. Arabian Journal of Geosciences 15, 1671. Available at: https://doi.org/10.1007/s12517-022-10941-6

Albanai, J.A., Mahamat, A.A., Abdelfatah, S.A., 2022b. Geostatistical analysis of natural oil seepage using radar imagery—a case study in Qaruh Island, the State of Kuwait. Arabian Journal of Geosciences 15, 469. Available at: https://doi.org/10.1007/s12517-022-09689-w

Al-naimi, N., Raitsos, D.E., Ben-hamadou, R., Soliman, Y., 2017. Evaluation of Satellite Retrievals of Chlorophyll- a in the Arabian Gulf 301, 1–13. Available at: https://doi.org/10.3390/rs9030301

Al-Rashidi, T.B., El-Gamily, H.I., Amos, C.L., Rakha, K.A., 2009. Sea surface temperature trends in Kuwait Bay, Arabian Gulf. Natural Hazards 50, 73–82. Available at: https://doi.org/10.1007/s11069-008-9320-9

Alyamani, F., Bishop, J., Ramadhan, E., Al-Husaini, M., Al-Ghadban, A., 2004. Oceanographic Atlas of Kuwait's waters, 1st ed. KISR.

Al-Yamani, F., Naqvi, S.W.A., 2019. Chemical oceanography of the Arabian Gulf. Deep Sea Research Part II: Topical Studies in Oceanography 161, 72–80. Available at: https://doi.org/10.1016/j.dsr2.2018.10.003

Al-Yamani, F., Saburova, M., Polikarpov, I., 2012. A preliminary assessment of harmful algal blooms in Kuwait's marine environment. Aquat Ecosyst Health Manag 15, 64–72. Available at: https://doi.org/10.1080/14634988.2012.679450

Brewer, P.G., Dyrssen, D., 1985. Chemical Oceanography of the Persian Gulf. Prog. Oeeanog 14, 41–55.

Brewin, R.J.W., Raitsos, D.E., Pradhan, Y., Hoteit, I., 2013. Comparison of chlorophyll in the Red Sea derived from MODIS-Aqua and in vivo fluorescence. Remote Sens Environ 136, 218–224. Available at: https://doi.org/10.1016/j.rse.2013.04.018

Cahyono, Agung.B., Armono, Haryo.D., Saptarini, D., 2017. Estimation of Sea Surface Temperature (SST) Using Split Window Methods for Monitoring Industrial Activity in Coastal Area. Trans Tech Publications, Switzerland Submitted: 862, 90–95. Available at: https://doi.org/10.4028/www.scientific.net/AMM.862.90

Chaplot, V., Darboux, F., Bourennane, H., Leguédois, S., Silvera, N., Phachomphon, K., 2006. Accuracy of interpolation techniques for the derivation of digital elevation models in relation to landform types and data density. Geomorphology 77, 126–141. Available at: https://doi.org/10.1016/j.geomorph.2005.12.010

Coleman, D., 2015. Mann Whitney Testing with Minitab [WWW Document]. URL Available at: https://www.leansigmacorporation.com/mann-whitney-testing-with-minitab/ (accessed 5.12.20).

D'Alimonte, D., Zibordi, G., 2003. Phytoplankton determination in an optically complex coastal region using a multilayer perceptron neural network. IEEE Transactions on Geoscience and Remote Sensing 41, 2861–2868. Available at: https://doi.org/10.1109/TGRS.2003.817682

Dames, Moore, 1983. Aquatic biology investigations. Studies for Sabiya area, Kuwait Bay and development of electrical networks. Kuwait.

Doney, S.C., 2006. Plankton in a warmer world. Nature 444, 695–696. Available at: https://doi.org/10.1038/444695a

El-Baz, F., Al-Sarawi, M., 2000. Atlas of State of Kuwait From Satellite Images, 1st ed. Kuwait Foundation for the Advancement of Sciences (KFAS).

Feldman, G.C., 2020a. Chlorophyll a (chlor_a) [WWW Document]. Nasa. URL Available at: https://oceancolor.gsfc.nasa.gov/atbd/chlor_a/ (accessed 9.30.20).

Feldman, G.C., 2020b. Suomi-NPP/VIIRS [WWW Document]. Nasa. URL oceancolor.gsfc.nasa.gov/data/viirs-snpp/ (accessed 9.30.20).

Gallegos, S.C., Lewis, M.D., Gould, R.W., Jr., Lawson, A., Amin, R., Gallegos, S.C., Ladner, S., 2015. Ocean Color Data Products over the Chesapeake Bay. Remote Sens (Basel) 7, 2193–2207. Available at: https://doi.org/10.3390/rs70202193

Glibert, P.M., Landsberg, J.H., Evans, J.J., Al-Sarawi, M.A., Faraj, M., Al-Jarallah, M.A., Haywood, A., Ibrahem, S., Klesius, P., Powell, C., Shoemaker, C., 2002. A fish kill of massive proportion in Kuwait Bay, Arabian Gulf, 2001: the roles of bacterial disease, harmful algae, and eutrophication. Harmful Algae 1, 215–231. Available at: https://doi.org/10.1016/S1568-9883(02)00013-6

Hattab, T., Jamet, C., Sammari, C., Lahbib, S., 2013. Validation of chlorophyll-α concentration maps from Aqua MODIS over the Gulf of Gabes (Tunisia): comparison between MedOC3 and OC3M bio-optical algorithms. Int J Remote Sens 34, 7163–7177. Available at: https://doi.org/10.1080/01431161.2013.815820

Hayase, K., Shinozuka, N., 1995. Vertical distribution of fluorescent organic matter along with AOU and nutrients in the equatorial Central Pacific. Mar Chem 48, 283–290. Available at: https://doi.org/10.1016/0304-4203(94)00051-E

Hu, C., Lee, Z., Franz, B., 2012. Chlorophyll a algorithms for oligotrophic oceans : A novel approach based on three-band reflectance difference. J Geophys Res 117, 1–25. Available at: https://doi.org/10.1029/2011JC007395

Huang, S., Lin, J., Lo, Y., Kuo, N., Ho, C., 2014. The coastal sea surface temperature changes near the nuclear power plants of northern Taiwan observed from satellite images. Oceans 2014 2–6.

Hunter, J.R., 1983. The physical oceanography of the Arabian Gulfs: a review and theoretical interpretation of previous observations, in: Marine Environment and Pollution, Proceedings of the First Arabian Gulf Conference on Environment and Pollution. Kuwait, pp. 1–23.

Husar, R.B., Prospero, M., Stowe, L.L., 1997. Characterization of tropospheric aerosols over the oceans with the NOAA advanced very high resolution radiometer optical thickness operational product. JOURNAL QF GEOPHYSICAL RESEARCH 102, 16889–16909.

Jensen, J.R., 2016. Introductory Digital Image Processing "A Remote Sensing Perspective," 4th ed. Prentice Hall Press.

Johns, W.E., Yao, F., Olson, D.B., 2003. Observations of seasonal exchange through the Straits of Hormuz and the inferred heat and freshwater budgets of the Persian Gulf. J Geophys Res 108, 3391. Available at: https://doi.org/10.1029/2003JC001881

Kahru, M., Kudela, R.M., Anderson, C.R., Manzano-Sarabia, M., Mitchell, B.G., 2014. Evaluation of satellite retrievals of ocean chlorophyll-a in the california current. Remote Sens (Basel) 6, 8524–8540. Available at: https://doi.org/10.3390/rs6098524

Kvenvolden, K.A., Cooper, C.K., 2003. Natural seepage of crude oil into the marine environment. Geo-Mar Lett 140–146. Available at: https://doi.org/10.1007/s00367-003-0135-0

Marrari, M., Hu, C., Daly, K., 2006. Validation of SeaWiFS chlorophyll a concentrations in the Southern Ocean: A revisit. Remote Sens Environ 105, 367–375. Available at: https://doi.org/10.1016/j.rse.2006.07.008

Mendonça, A.P., Martins, A.M., Figueiredo, M.P., Bashmachnikov, I.L., Couto, A., Lafon, V.M., Aristegui, J., 2010. Evaluation of ocean color and sea surface temperature sensors algorithms using in situ data: a case study of temporal and spatial variability on two northeast Atlantic seamounts. J Appl Remote Sens 4, 1–26. Available at: https://doi.org/10.1117/1.3328872

Misak, R., Mahfoz, S., Alasfour, T., 2003. Desert Environment on The State of Kuwait. Center For Research and Studies on Kuwait.

Moradi, M., Kabiri, K., 2015. Spatio-temporal variability of SST and Chlorophyll-a from MODIS data in the Persian Gulf. Mar Pollut Bull 98, 14–25. Available at: https://doi.org/10.1016/j.marpolbul.2015.07.018

Moradi, M., Kabiri, K., 2012. Red tide detection in the Strait of Hormuz (east of the Persian Gulf) using MODIS fluorescence data. Int J Remote Sens 33, 1015–1028. Available at: https://doi.org/10.1080/01431161.2010.545449

Muller-Karger, F.E., Hu, C., Andréfouët, S., Varela, R., Thunell, R., 2005. The Color of the Coastal Ocean and Applications in the Solution of Research and Management Problems, in: Miller, R.L., Del Castillo, C.E., Mckee, B.A. (Eds.), Remote Sensing of Coastal Aquatic Environments: Technologies, Techniques and Applications. Springer Netherlands, Dordrecht, pp. 101–127. Available at: https://doi.org/10.1007/978-1-4020-3100-7_5

Musashi, J.P., Pramoedyo, H., Fitriani, R., 2018. Comparison of Inverse Distance Weighted and Natural Neighbor Interpolation Method at Air Temperature Data in Malang Region. CAUCHY – JURNAL MATEMATIKA MURNI DAN APLIKASI 5, 48–54.

Mutlow, C.T., Zavody, A.M., Barton, I.J., Llewellyn-Jones, D.T., 1994. Sea surface temperature measurements by the along-track scanning radiometer on the ERS 1 satellite: early results. J Geophys Res 99, 22,522-575,588.

Nezlin, N.P., Polikarpov, I.G., Al-yamani, F., 2007. Satellite-measured chlorophyll distribution in the Arabian Gulf : Spatial , seasonal and inter-annual variability. International Journal of Oceans and Oceanography 2, 139–156.

Nezlin, N.P., Polikarpov, I.G., Al-Yamani, F.Y., Subba Rao, D. V, Ignatov, A.M., 2010. Satellite monitoring of climatic factors regulating phytoplankton variability in the Arabian (Persian) Gulf. Journal of Marine Systems 82, 47–60. Available at: https://doi.org/10.1016/j.jmarsys.2010.03.003

O'Reilly, J.E., Maritorena, S., Mitchell, B.G., Siegel, D.A., Carder, K.L., Garver, S.A., Kahru, M., McClain, C., 1998. Ocean color chlorophyll algorithms for SeaWiFS. J Geophys Res Oceans 103, 24937–24953. Available at: https://doi.org/10.1029/98JC02160

Pokavanich, T., Alosairi, Y., Graaff, R. de, Morelissen, R., Verbruggen, W., Al-Refail, K., Taqi, A., Al-Said, T., 2014. THREE-DIMENSIONAL HYDRO-ENVIRONMENT CHARACTERIZATION AND MODELING OF THE NORTHERN ARABIAN GULF. Coastal Engineering Proceedings. Available at: https://doi.org/10.9753/icce.v34.management.41

Polikarpov, I., Al-yamani, F., Saburova, M., 2019. Remote Sensing of Phytoplankton Variability in the Arabian / Persian Gulf, in: Barale, V., Gade, M. (Eds.), Remote Sensing of the Asian Seas. Springer, pp. 485–501. Available at: https://doi.org/10.1007/978-3-319-94067-0

Polikarpov, I., Saburova, M., Al-Yamani, F., 2016. Diversity and distribution of winter phytoplankton in the Arabian Gulf and the Sea of Oman. Cont Shelf Res 119, 85–99. Available at: https://doi.org/10.1016/j.csr.2016.03.009

Reilly, J., O'Brien, M., Siegel, D., Toole, D., Menzies, D., Smith, R., Mueller, J., Mitchell, B., Kahru, M., Chavez, F., Strutton, P., Cota, G., Mcclain, C., Carder, K., Harding, L., Magnuson, A., Phinney, D., Culver, M., 2000. SeaWiFS Postlaunch Calibration and Validation Analyses, Part 3.

Reynolds, R.M., 1993. Physical oceanography of the Gulf, Strait of Hormuz, and the Gulf of Oman—Results from the Mt Mitchell expedition. Mar Pollut Bull 27, 35–59.

Shang, S.L., Dong, Q., Hu, C.M., Lin, G., Li, Y.H., Shang, S.P., 2014. On the consistency of MODIS chlorophyll a products in the northern South China Sea. Biogeosciences 11, 269–280. Available at: https://doi.org/10.5194/bg-11-269-2014

Sheppard, C., Al-husiani, M., Al-jamali, F., Al-yamani, F., Baldwin, R., Bishop, J., Benzoni, F., Dutrieux, E., Dulvy, N.K., Rao, S., Durvasula, V., Jones, D.A., Loughland, R., Medio, D., Nithyanandan, M., Pilling, G.M., Polikarpov, I., Price, A.R.G., Purkis, S., Riegl, B., Saburova, M., Samimi, K., Taylor, O., Wilson, S., Zainal, K., 2010. The Persian / Arabian Gulf : a young sea in decline . Mar Pollut Bull The Gulf : A young sea in decline q. Mar Pollut Bull 60, 13–38. Available at: https://doi.org/10.1016/j.marpolbul.2009.10.017

Siegel, D.A., Maritorena, S., Nelson, N.B., Behrenfeld, M.J., McClain, C.R., 2005. Colored dissolved organic matter and its influence on the satellite-based characterization of the ocean biosphere. Geophys Res Lett 32, 1–4. Available at: https://doi.org/10.1029/2005GL024310

Sunda, W., 2012. Feedback Interactions between Trace Metal Nutrients and Phytoplankton in the Ocean. Front Microbiol 3, 204. Available at: https://doi.org/10.3389/fmicb.2012.00204

Thomas, A., Byrne, D., Weatherbee, R., 2002. Coastal sea surface temperature variability from Landsat infrared data. Remote Sens Environ 81, 262–272. Available at: https://doi.org/10.1016/S0034-4257(02)00004-4

Watson, D.F., Philip, G.M., 1985. A Refinement of Inverse Distance Weighted Interpolation. Geoprocessing 2, 315–327.

Williams, G.N., Dogliotti, A.I., Zaidman, P., Solis, M., Narvarte, M.A., González, R.C., Esteves, J.L., Gagliardini, D.A., 2013. Assessment of remotely-sensed sea-surface temperature and chlorophyll-a concentration in San Matías Gulf (Patagonia, Argentina). Cont Shelf Res 52, 159–171. Available at: https://doi.org/10.1016/j.csr.2012.08.014

Willmott, C.J., 1981. ON THE VALIDATION OF MODELS. Phys Geogr 2, 184–194. Available at: https://doi.org/10.1080/02723646.1981.10642213

Wirasatriya, A., Kunarso, Maslukah, L., Satriadi, A., Armanto, R.D., 2018. Different responses of chlorophyll-a concentration and Sea Surface Temperature (SST) on southeasterly wind blowing in the Sunda Strait, in: IOP Conf. Series: Earth and Environmental Science 139. IOP Publishing, pp. 1–7. Available at: https://doi.org/10.1088/1755-1315/139/1/012028

Yoder, J.A., O'Reilly, J.E., Barnard, A.H., Moore, T.S., Ruhsam, C.M., 2001. Variability in coastal zone color scanner (CZCS) Chlorophyll imagery of ocean margin waters off the US East Coast. Cont Shelf Res 21, 1191–1218. Available at: https://doi.org/10.1016/S0278-4343(01)00009-7

Zhang, C., Hu, C., Shang, S., Müller-Karger, F.E., Li, Y., Dai, M., Huang, B., Ning, X., Hong, H., 2006. Bridging between SeaWiFS and MODIS for continuity of chlorophyll-a concentration assessments off Southeastern China. Remote Sens Environ 102, 250–263. Available at: https://doi.org/10.1016/j.rse.2006.02.015

Zhang, Y., Jiang, H., Chen, C., Zhang, X.Y., Wang, Y., 2012. Wavelet analysis on chlorophyll concentration change in the area around Bohai Bay area, Yangtze River Delta Region and South China Sea. Procedia Environ Sci 13, 1373–1382. Available at: https://doi.org/10.1016/j.proenv.2012.01.130

Zhao, J., Ghedira, H., 2014. Monitoring red tide with satellite imagery and numerical models: A case study in the Arabian Gulf. Mar Pollut Bull 79, 305–313. Available at: https://doi.org/10.1016/j.marpolbul.2013.10.057

Zhao, J., Temimi, M., Kitbi, S. Al, Mezhoud, N., 2016. Monitoring HABs in the shallow Arabian Gulf using a qualitative satellite- based index. Int J Remote Sens 37, 1937–1953. Available at: https://doi.org/10.1080/01431161.2016.1165886